

# Redshift remapping and cosmic acceleration in dark-matter-dominated cosmological models

Radosław Wojtak<sup>1,2\*</sup> and Francisco Prada<sup>1,3,4,5</sup>

<sup>1</sup>*Kavli Institute for Particle Astrophysics and Cosmology, Stanford University, SLAC National Accelerator Laboratory, Menlo Park, CA 94025, USA*

<sup>2</sup>*Dark Cosmology Centre, Niels Bohr Institute, University of Copenhagen, 2100 Copenhagen Ø, Denmark*

<sup>3</sup>*Instituto de Física Teórica, (UAM/CSIC), Universidad Autónoma de Madrid, Cantoblanco, E-28049 Madrid, Spain*

<sup>4</sup>*Campus of International Excellence UAM+CSIC, Cantoblanco, E-28049 Madrid, Spain*

<sup>5</sup>*Instituto de Astrofísica de Andalucía, (IAA/CSIC), Glorieta de la Astronomía, E-18190 Granada, Spain*

28 June 2017

## ABSTRACT

The standard relation between the cosmological redshift and cosmic scale factor underlies cosmological inference from virtually all kinds of cosmological observations, leading to the emergence of the  $\Lambda$  cold-dark-matter ( $\Lambda$ CDM) cosmological model. This relation is not a fundamental theory and thus observational determination of this function (redshift remapping) should be regarded as an insightful alternative to holding its standard form in analyses of cosmological data. Here we present non-parametric reconstructions of redshift remapping in dark-matter-dominated models and constraints on cosmological parameters from a joint analysis of all primary cosmological probes including the local measurement of the Hubble constant, Type Ia supernovae, baryonic acoustic oscillations (BAO), Planck observations of the cosmic microwave background (CMB) radiation (temperature power spectrum) and cosmic chronometers. The reconstructed redshift remapping points to an additional boost of redshift operating in late epoch of cosmic evolution, but affecting both low-redshift observations and the CMB. The model predicts a significant difference between the actual Hubble constant,  $h = 0.48 \pm 0.02$ , and its local determination,  $h_{\text{obs}} = 0.73 \pm 0.02$ . The ratio of these two values coincides closely with the maximum expansion rate inside voids formed in the corresponding open cosmological model with  $\Omega_{\text{m}} = 0.87 \pm 0.03$ , whereas the actual value of the Hubble constant implies the age of the Universe that is compatible with the Planck  $\Lambda$ CDM cosmology. The model with redshift remapping provides excellent fits to all data and eliminates recently reported tensions between the Planck  $\Lambda$ CDM cosmology, the local determination of the Hubble constant and the BAO measurements from the Ly- $\alpha$  forest of high-redshift quasars.

**Key words:** cosmology: observations, distance scale, cosmological parameters – methods: statistical

## 1 INTRODUCTION

Compelling observational evidences demonstrate that the Universe is undergoing a phase of accelerated expansion. The accelerated expansion manifests itself in various observations probing different aspects of cosmic evolution, from observations of Type Ia supernovae (Perlmutter et al. 1999; Riess et al. 1998), through observations of the cosmic microwave background (CMB) radiation (Planck Collaboration et al. 2016b) and the abundance of galaxy clusters (Mantz et al. 2015). These vast observational data laid the foundation of the concordance cosmological model in which

all observational signatures of cosmic acceleration are reconciled with the theoretical predictions of general relativity by introducing a positive cosmological constant  $\Lambda$ . The great success of the resulting standard  $\Lambda$  cold dark matter ( $\Lambda$ CDM) model can be appreciated by realizing that the model is capable of reducing information contained in all cosmological observations to a set of only six parameters including the cosmological constant.

Despite its simplicity and capacity to describe key cosmological data, the  $\Lambda$ CDM model lacks fundamental understanding of its main constituents. In particular, the cosmological constant making up nearly 70 % of the total energy budget in the Universe (Planck Collaboration et al. 2016b) cannot be explained on the ground of well-

\* E-mail: wojtak@stanford.edu, f.prada@csic.es

established physics. It has been long known that its only viable interpretation as the vacuum energy results in the largest discrepancy between observations and theory which predicts its energy density exceeding the observational determinations by  $\sim 120$  orders of magnitude (Carroll 2001).

After two decades of intense data-driven progress in cosmology, the physical nature of cosmic acceleration remains unknown and becomes arguably the most challenging mystery of modern cosmology. Many ongoing and upcoming cosmological surveys such as the Dark Energy Survey (DES) (The Dark Energy Survey Collaboration 2005), Euclid (Laureijs et al. 2011), the Dark Energy Spectroscopic Instrument (DESI) (Levi et al. 2013) or the Large Synoptic Survey Telescope (LSST) (LSST Dark Energy Science Collaboration 2012) are devised to shed light on this problem. This observational strategy, however, does not seem to be fully balanced by concept-driven paths of research. In particular, the main effort focused on observational determination of dark energy equation state assumes implicitly the existence of dark energy and excludes the possibility that cosmic acceleration may be an emergent phenomenon of yet unknown physical nature. The best example of the latter possibility is a modification of gravity such as  $f(R)$  gravity (Clifton & Dunsby 2015). This approach accounts for cosmic acceleration by modifying the Einstein's equations rather than by postulating the existence of an additional form of energy. This scenario is seriously considered as a viable alternative to dark energy, although most models of modified gravity must closely mimic the cosmological constant in order not to violate stringent tests of gravity on scales of the Solar System (Brax et al. 2008; Ceron-Hurtado et al. 2016). Yet, it does not exhaust all possibilities for exploring the problem of cosmic acceleration as an emergent phenomenon.

Necessity of considering models going beyond the boundaries of the standard  $\Lambda$ CDM cosmology stems from gradually increasing observational anomalies. Arguably two most alarming tensions within the standard cosmological model include discrepancy between the local and the CMB-based Planck determination of the Hubble constant (Bernal et al. 2016), and anomalous values of the baryonic acoustic oscillations (BAO) determined from the Ly- $\alpha$  forest of high-redshift quasars observed in the SDSS-III/BOSS (Sloan Digital Sky Survey/Baryon Oscillations Spectroscopic Survey) (Font-Ribera et al. 2014; Delubac et al. 2015). These two tensions are recognized at a moderate-strong confidence level of  $\sim 3\sigma$ . However, if they are corroborated by future observations the standard model will need to undergo a substantial change in order to absorb both anomalies. The tension in the measurements of the Hubble constant would require a phantom-like dark energy (Di Valentino et al. 2016), whereas the BAO anomaly could be solved by employing models with evolving dark energy (Sahni et al. 2014). Such modifications would diminish arguably appealing simplicity of the  $\Lambda$ CDM model and reinforce the motivation for exploring other theoretical propositions leading potentially to understanding of the cosmic acceleration phenomenon.

The property of cosmic acceleration is a necessary element in reconciling observations with the assumed theoretical framework. Different layers of this framework, however, can effectively play the same role in the process of establishing a concordance model. Considering two contrasting ex-

amples, cosmic acceleration can be ascribed either to dark energy or a new form of gravity. Less obvious layer of the framework involves the computation of cosmological observables. On one hand, this layer is expected to be fully specified by the assumed model of gravity. On the other hand, it may strongly depend on the accuracy of adopted approximate solutions. This problem of potentially inaccurate models of cosmological observables concern the standard cosmological model based on a fully isotropic and homogenous metric, the Friedmann-Lemaître-Robertson-Walker (FLRW) metric, for which potentially large differences between its derivatives and the corresponding derivatives of the actual metric of the Universe may result in significant discrepancies between observations and their models (Green & Wald 2014). With the recent advent of fully relativistic cosmological simulations (Bentivegna & Bruni 2016; Giblin et al. 2016), we just begin to address this long-standing problem in a fully rigorous way.

The primary effect of cosmic evolution on light propagation is the cosmological redshift. In the standard theoretical framework underlying essentially all interpretations of cosmological data, the cosmological redshift is a theoretically assumed function of the scale factor, derived from the FLRW metric. This function, however, may not necessarily comply with the actual mapping between the cosmological redshift and cosmic scale factor. As shown by Bassett et al. (2013) and Wojtak & Prada (2016), one can therefore attempt to reconstruct this mapping from observations rather than to postulate its theoretical form. In order to differentiate it from the standard relation between the cosmological redshift  $z$  and cosmic scale factor  $a$ , we shall hereafter refer to observationally reconstructed  $a-z$  relation as redshift remapping. Fig. 1 demonstrates a geometric representation of this idea in space spanned by cosmic time, cosmic scale factor and the cosmological redshift. The red plane contains all theoretical models with the standard mapping between cosmic scale factor and the cosmological redshift ( $1+z=1/a$ ), i.e. with the same projection onto the  $a-z$  plane. Cosmological observations reduce possible solutions to a line whose projection onto the  $a-t$  plane is the expansion history of the standard  $\Lambda$ CDM model. Including redshift remapping as an additional degree of freedom opens up new space of models. As shown in our recent work (Wojtak & Prada 2016), observational constraints on redshift remapping from low-redshift probes, including Type Ia supernovae and BAO, are degenerated with the dark energy density parameter. Therefore, the new cosmological models with redshift remapping form a 2D manifold of models (the blue surface in Fig. 1) with different combinations of dark energy (expansion history) and redshift remapping. In the context of cosmic acceleration, of particular interest is the model dominated by dark matter (without dark energy) in which the observationally determined redshift remapping accounts for cosmic acceleration. In the above description, the 2D manifold is an idealized representation of the posterior probability distribution which would effectively gives rise to a small thickness of this surface. Without loss of generality, this idealization is made for the sake of clarity of demonstrating new cosmological inference with redshift remapping.

The current cosmological models with redshift remapping are phenomenological in a sense that the  $a-z$  relation is constrained by observations amongst standard cosmolog-

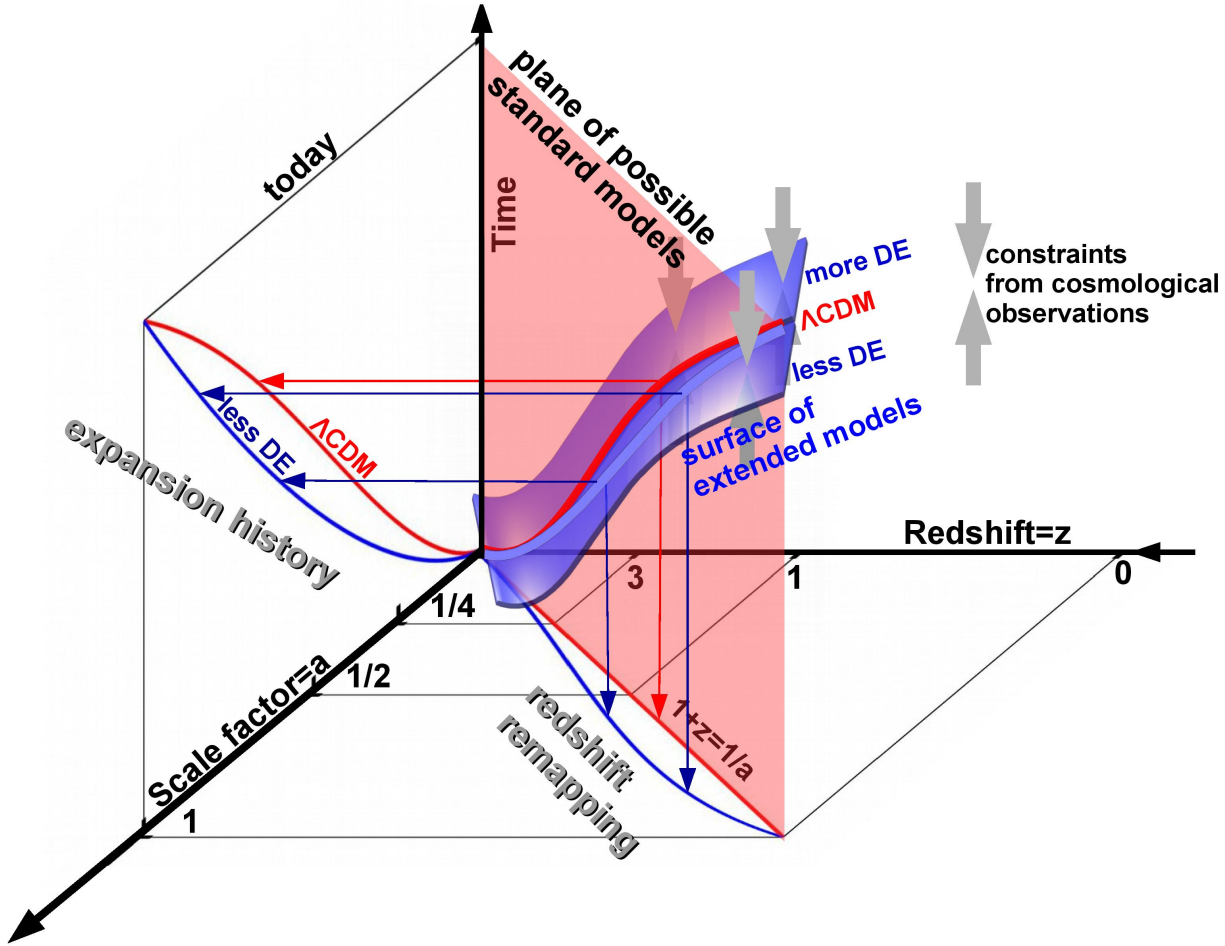


**Figure 1.** Conceptual scheme of cosmological models with redshift remapping. The standard approach assumes that mapping between the cosmological redshift  $z$  and the scale factor  $a$  is given by  $1+z=1/a$ . Therefore, standard theoretical models are always confined strictly to the red plane in 3D space spanned by redshift, cosmic scale factor and time. Redshift remapping (non-standard relation between cosmic scale factor and the cosmological redshift) violates this restriction and the resulting models populate space around the red plane. Cosmological observations constrain, however, the allowed space to a 2D manifold (the blue surface between the grey arrows representing constraints from cosmological data). Every model is represented by a line whose projections onto the  $a-t$  and  $a-z$  planes show respectively the expansion history and redshift remapping of the underlying model. Models in front of the red plane require less dark energy than the standard  $\Lambda$ CDM and  $1+z > 1/a$  (see an example shown by the blue line), whereas models behind the red plane are characterized by higher dark energy content and  $1+z < 1/a$ . The intersection of the blue surface with the red plane is a  $\Lambda$ CDM model with  $1+z=1/a$ .

ical parameters. However, there clearly exists a potential for theoretical considerations. Non-trivial redshift remapping can emerge both in non-metric theories of gravity such as  $\delta$  gravity (Alfaro 2012; Alfaro & González 2013) and many general-relativistic models going beyond the standard FLRW cosmology, e.g. the Lindquist-Wheeler model with a discretized matter content (Clifton & Ferreira 2009; Clifton et al. 2012), conformal FLRW cosmologies (Visser 2015), models with non-linear inhomogeneities (see e.g. Meures & Bruni 2012; Lavinto et al. 2013). The latter group of models is probably much broader. We enumerate only selected examples for which a deviation of the  $a-z$  relation from its standard form was explicitly shown.

The main goal of this paper is to improve the results presented in (Wojtak & Prada 2016) by combining all relevant low-redshift probes and CMB observations in a joint

analysis of models with redshift remapping. Including CMB data not only improves observational constraints, but it also allows for revisiting anomalies in the Hubble constant determinations and the BAO observations in the context of new cosmological models with redshift remapping. In addition, we develop a new method which allows for a non-parametric reconstruction of redshift remapping from observations. The new method replaces a simplified parametric approach employed in (Wojtak & Prada 2016). We limit our analysis to the most interesting case of dark-matter-dominated models without dark energy. Therefore, the final constraints on cosmological parameters and redshift remapping establish an alternative model in which cosmic acceleration emerges exclusively from a new phenomenological mapping between the cosmological redshift and cosmic scale factor.

The manuscript is organized as follows. In section 1, we

introduce the idea of redshift remapping and describe a new approach to its observational determination based on a non-parametric fitting. In section 2, we outline the framework for computing all relevant observables in cosmological models with redshift remapping. Next, we describe cosmological data used in this work. In section 3, we present observational constraints on cosmological parameters and redshift remapping. Then we discuss all results in section 4 and summarize in section 5.

## 2 REDSHIFT REMAPPING

Extragalactic redshifts in the CMB rest frame  $z_{\text{obs}}$  can be factorized into the contributions from expansion of space along the photon path  $z_s$  and the peculiar velocity of the emitter in the following way

$$1 + z_{\text{obs}} = (1 + z_s)(1 + v_{\text{pec}}/c), \quad (1)$$

where  $v_{\text{pec}}$  is the projection of the peculiar velocity onto the line of sight of the observer. Without loss of generality, we assume here that our observations do not include objects with strong gravity such as black holes and we also neglect higher order relativistic corrections from large scale structures such as gravitational redshift (although imprints of these effects are already detectable in the current cosmological surveys, see (Wojtak et al. 2011; Jimeno et al. 2015; Sadeh et al. 2015)). Peculiar velocities play important role in the interpretation of the observation of the local Universe where measured redshifts are of comparable magnitude to Doppler shifts due to peculiar velocities. However, in many cases of high redshift observations their contribution can be neglected and the observed redshift  $z_{\text{obs}}$  can be identified with  $z_s$ . This approach is fully justified when the only effect of peculiar velocities is to give rise an additional scatter in multiple measurements around a relation between a cosmological observable and  $z_s$  (for example, the Hubble diagram for Type Ia supernovae) or when the effect vanishes as a result of averaging in redshift bins (for example, redshift bins of BAO measurements). Since all data sets used in our work fall into one of the two above categories, we hereafter assume  $z_{\text{obs}} = z_s$ , as it is customary to proceed in all standard cosmological analyses unless the peculiar velocity field itself is an observable.

Cosmological observations constrain in general theoretical relations between various cosmological observables and the cosmological redshift  $z_{\text{obs}}$  which reflects the expansion of space integrated along the photon path. Utilizing these observations to determine the expansion history and the contents of the Universe requires two assumptions: the mapping between  $z_{\text{obs}}$  and the scale factor  $a$  describing global evolution of cosmic space and an equation relating time evolution of cosmic scale factor  $a(t)$  to the energy-matter contents of the Universe. Within the standard cosmological framework, both relations are derived assuming a fully isotropic and homogeneous metric: the Friedmann-Lemaître-Robertson-Walker (FLRW) metric,

$$ds^2 = dt^2 - a(t)^2 \left( \frac{dr^2}{1 - kr^2} + r^2 d\Omega \right), \quad (2)$$

where  $k = \pm 1, 0$ . The mapping between  $a$  and  $z_{\text{obs}}$  in this case is reduced to the well-known expression

$$1 + z_{\text{obs}} = \frac{1}{a} \quad (3)$$

and the time evolution of the scale factor is governed by the Friedmann equation, i.e.

$$\left( \frac{\dot{a}}{a} \right)^2 / H_0^2 \equiv \frac{H^2}{H_0^2} = \Omega_{\text{R}} a^{-4} + \Omega_{\text{m}} a^{-3} + \Omega_{\text{K}} a^{-2} + \Omega_{\Lambda}, \quad (4)$$

where  $H \equiv \dot{a}/a$  is the Hubble parameter and  $H_0$  is the Hubble constant today when  $a \equiv 1$ .  $\Omega_{\text{R}}$ ,  $\Omega_{\text{m}}$ ,  $\Omega_{\text{K}}$ , and  $\Omega_{\Lambda}$  are the radiation, matter (both cold and baryonic), spatial curvature and cosmological constant density parameters.

The key notion of our model was introduced in (Bassett et al. 2013; Wojtak & Prada 2016) and is based on the realization that the mapping between the scale factor  $a$  and the cosmological redshift  $z_{\text{obs}}$  does not have to be a necessary assumption in cosmological inference, but instead can be observationally determined, simultaneously with other relevant cosmological parameters. It is quite intuitive to expect that the empirically motivated  $a - z_{\text{obs}}$  mapping should not deviate significantly from the standard mapping given by equation (3). It is therefore reasonable to quantify the new mapping as a relative correction to the standard relation based on the FLRW metric. Following (Bassett et al. 2013) and (Wojtak & Prada 2016), we use the ratio of the redshift inferred from the FLRW metric to the actually observed redshift

$$\frac{z_{\text{FLRW}}}{z_{\text{obs}}} \equiv \frac{1/a - 1}{z_{\text{obs}}} = 1 + \alpha(z_{\text{obs}}), \quad (5)$$

where

$$1 + z_{\text{FLRW}} \equiv \frac{1}{a}. \quad (6)$$

and  $\alpha(z_{\text{obs}})$  is a free function of  $z_{\text{obs}}$ . Using the above ratio of the two redshifts allows to avoid an unphysical situation with non-vanishing  $z_{\text{FLRW}}$  redshifts at distances approaching 0. For any finite value of  $\alpha$  at  $z_{\text{obs}} = 0$ ,  $z_{\text{obs}} = 0$  implies vanishing  $z_{\text{FLRW}}$ .

The function  $\alpha(z_{\text{obs}})$  in equation (5) describes a relative difference between the standard mapping given by equation (3) and observationally motivated mapping between the scale factor and the observed redshift  $z_{\text{obs}}$ . Hereafter we shall refer to the latter as *redshift remapping*. The standard mapping and redshift remapping become identical when  $\alpha(z_{\text{obs}}) = 0$ .

Every mapping between the scale factor and the observed redshift is always ascribed to gravity and the metric which determine propagation of photons. Therefore, redshift remapping can emerge either from differences between the true metric of the Universe and the FLRW approximation or from violation of the principle describing photon paths as null geodesic lines in spacetime. As we shall see in the following section, the way how we calculate all cosmological observables in our model *excludes the possibility of interpreting redshift remapping as a non-metric-based effect* such as Zwicky's hypothesis of 'tired light'. This important property allows us to comply with cosmological observations ruling out non-metric-based origin of cosmological redshifts, e.g. redshift dependence of the spectral aging rate of Type Ia supernovae (Blondin et al. 2008) or blackness of the CMB spectral energy distribution (Ellis et al. 2013).

## 2.1 Parametrization

The main difficulty of constraining redshift remapping lies in the fact that it employs an unknown function  $\alpha(z_{\text{obs}})$  that increases substantially the degrees of freedom of cosmological fits. As an attempt to resolve this problem (Bassett et al. 2013) proposed simple parametrizations based on Taylor expansion of  $\alpha(z_{\text{obs}})$  and (Wojtak & Prada 2016) used a well-motivated but simplistic ansatz for redshift remapping. Although both approaches can give many interesting insights into cosmological fits with redshift remapping, they do not provide a complete solution of the problem. In particular, they do not allow to constrain the shape of redshift remapping.

The best available technique which can be used to reconstruct the full shape of redshift remapping from observations is a non-parametric fit. Here we describe several technical details how we implement this technique in our analysis.

The current cosmological data including observations of Type Ia supernovae and BAO allow us to probe redshift remapping in the redshift range from  $z_{\text{obs}} = 0$  to  $z_{\text{obs}} \approx 2.5$ . The upper limit comes from the BAO measurements based on observations of the Ly- $\alpha$  forest of high-redshift SDSS-III/BOSS quasars. A non-parametric fit relies on approximating an unknown function by a set of its values at several points of an independent variable and adopting an interpolation scheme for evaluating the function between these points. Performing a series of trial fits, we found that the most optimized set-up for a non-parametric reconstruction of redshift remapping employs spline interpolation between four redshifts given by  $z_{\text{obs}} = 0, 0.5, 1.0, 2.5$ . The last redshift bin includes both high redshift supernovae, Hubble parameter from cosmic chronometers and the BAO measurements from observations of the Ly- $\alpha$  forest of BOSS quasars. Redshift remapping  $\alpha(z_{\text{obs}})$  is therefore fully determined by 6 parameters: 4 values of  $\alpha(z_{\text{obs}})$  at the four redshifts  $z_{\text{obs}}$  used by the interpolation scheme and 2 values of derivative  $d\alpha(z_{\text{obs}})/dz_{\text{obs}}$  at  $z_{\text{obs}} = 0, 2.5$ . As a sanity check, we verified that our constraints on redshift remapping barely depend on the actual choice of binning adopted for the interpolation. In particular, changing the bin sizes or the position of the last bin keep the best-fitting profile of redshift remapping well within the error envelope of our main results. Moreover, increasing the number of bins does not reveal any additional and statistically significant features of the profile (see Fig. A1 in Appendix).

The employed technique of constraining redshift remapping allows in general for a number of solutions which can be rejected on the ground of expecting a relatively simple functional form of  $\alpha(z_{\text{obs}})$ . For example, oscillatory solutions or highly non-monotonic functions seem to be highly suspicious and, on the basis of the argument from simplicity, they should rather be ignored. To comply with this condition we narrow down the whole family of solutions by means of employing prior distributions on the six parameters determining redshift remapping. Our choice of the priors is motivated by the expected form of redshift remapping for dark-matter-dominated cosmological models considered in this work. As shown in (Wojtak & Prada 2016), redshift remapping in this case increases monotonically with redshift and  $1 + \alpha(z_{\text{obs}}) \leq 1$ . Adopting this property as a prior in our analysis leads to the following condition

$$\alpha(0) \leq \alpha(0.5) \leq \alpha(1.0) \leq \alpha(2.5) \leq 0. \quad (7)$$

As we shall see in the following section, the above inequality implies automatically monotonicity of the comoving distance as a function of redshift  $z_{\text{obs}}$ . However, they do not guarantee that the Hubble parameter as a function redshift is free of wiggle-like features. Therefore, as the second prior we require every model to comply with the condition that the Hubble parameter increases monotonically with redshift. This condition is tested numerically in every iteration of our cosmological fits. Due to the relatively weak constraining power of the data in the last redshift bin, we also narrow down the range of the first derivative of  $\alpha(z_{\text{obs}})$  at  $z_{\text{obs}} = 2.5$  to  $[0, 0.1]$ .

The CMB observations provide additional constraints on  $\alpha(z_{\text{obs}})$  at the redshift of the last scattering surface,  $z_{\text{obs}} \approx 1100$ . This measurement probes a single value of redshift remapping and it is independent of the constraints from low redshift probes (apart from the case of a joint analysis combining low-redshift and CMB data). Comparing constraints on  $\alpha(z_{\text{obs}})$  from low-redshift probes with its value at the last scattering surface can give some hints on the form of  $\alpha(z_{\text{obs}})$  in the redshift range without any data. For example, if the former indicates a clear convergence of  $\alpha(z_{\text{obs}})$  and its maximum value at  $z_{\text{obs}} < 2.5$  is consistent with redshift remapping determined from the CMB then one can likely expect the existence of a plateau extending between  $z_{\text{obs}} = 2.5$  and  $z_{\text{obs}} \approx 1100$ .

## 2.2 Background model

In order to close the system of equations underlying the framework for calculating all basic cosmological observables such as distances, we need to specify the equation governing the time evolution of the scale factor. Despite the fact that our approach modifies the standard mapping between the scale factor and the observed redshift – one of the direct predictions based on the FLRW metric, we keep the Friedmann equation given by (4) unchanged. Since we restrict our work to dark-matter-dominated cosmological models ( $\Omega_{\Lambda} \equiv 0$ ), the Friedman equation at redshifts characteristic for BAO and Type Ia supernova observations reads

$$\frac{(\dot{a}/a)^2}{H_0^2} \equiv \frac{H^2}{H_0^2} = \Omega_{\text{m}}(1 + z_{\text{FLRW}})^3 + (1 - \Omega_{\text{m}})(1 + z_{\text{FLRW}})^2. \quad (8)$$

Combining the Friedmann equation with a modification of the standard redshift remapping may not seem to form a self-consistent framework. This inconsistency is inevitable when we assume that the FLRW metric is accurate on all scales and general relativity is correct at least on large scales. However, this condition can be broken either due to inadequacy of the FLRW metric for describing the first derivatives of the actual metric of the Universe (Green & Wald 2014) or due to the violation of a general framework of relativity in which photons propagate along null geodesic lines. The former circumstance arises in many general-relativistic cosmological models whose global evolution is governed by the Friedmann equation, but whose observables cannot be accurately described with the FLRW metric (see e.g. Clifton & Ferreira 2009; Lavinto et al. 2013; Bentivegna & Bruni 2016). The key optical property undergoing substantial modification compared to the predictions

based on the FLRW metric is the mapping between the scale factor and the cosmological redshift.

Redshift remapping is a phenomenological model which does not attempt to incorporate any specific theoretical model predicting deviations from the standard mapping between the scale factor and the cosmological redshift based on the FLRW metric. Keeping the phenomenological status of our model allows us to be independent of any specific theoretical explanations of redshift remapping, no matter if they are related to the inadequacy of the FLRW metric or some modifications of general-relativistic principles of light propagation. However, due to its simplicity and the potential for a straightforward and systematic exploration, we tend to think of redshift remapping as a phenomenon emerging from differences between the true metric of the Universe and the FLRW approximation.

With the recent advent of fully relativistic cosmological simulations based on obtaining exact numerical solutions of the Einstein field equations (Bentivegna & Bruni 2016; Giblin et al. 2016), effects of structure formation on the actual metric can be studied in a much more rigorous way than before. Recent studies of such simulations demonstrated that non-linear evolution of cosmic structures induces strong inhomogeneities in the local expansion rate what is expected to have a non-negligible effect of the computation of observables, in particular the mapping between the cosmological redshift and cosmic scale factor. At the same time, the presence of such a locally inhomogeneous expansion appears to have a negligible impact on the global expansion of the Universe. Combining these two facts we can see that our new framework based on the Friedmann equation and redshift remapping can be fully consistent with general relativity. In this interpretation, redshift remapping is merely a theoretically unknown relation between the cosmological redshift and cosmic scale factor, which has yet to be established in upcoming advances of fully relativistic simulations.

### 3 OBSERVABLES

We calculate all cosmological observables assuming that redshift remapping is a purely metric-based effect. This assumption implies that the distance-duality relation with the observed redshift  $z_{\text{obs}}$  holds, even though  $z_{\text{obs}}$  can be different than  $z_{\text{FLRW}}$  (Meures & Bruni 2012),

$$D_L(z_{\text{obs}}) = (1 + z_{\text{obs}})^2 D_A(z_{\text{obs}}), \quad (9)$$

where  $D_L$  is the luminosity distance and  $D_A$  is the angular diameter distance. The relation follows directly from two fundamental principles: the conservation of photons and the so-called reciprocity theory (also known as Etherington's theory, (Etherington 1933)). Needless to say, the relation would be violated if  $(1 + z_{\text{obs}})$  factor was replaced by  $(1 + z_{\text{FLRW}})$ .

#### 3.1 Cosmological distances

We assume that the comoving distance  $D_M$  to an object observed at redshift  $z_{\text{obs}}$  is given by

$$D_M(z_{\text{obs}}) = c \int_0^{z_{\text{obs}}[1+\alpha(z_{\text{obs}})]} \frac{dz_{\text{FLRW}}}{H(z_{\text{FLRW}})}, \quad (10)$$

where  $H(x)$  is the Hubble parameter defined in equation (8). Compared to the standard formula based on the FLRW metric (see e.g. (Hogg 1999)), the only difference arising from redshift remapping concerns the upper limit of the integral which relates the observed redshift to the scale factor at the time of emission. The standard formula is recovered when  $\alpha(z_{\text{obs}})$  vanishes at all redshifts.

As a consequence of the distance-duality relation, redshift remapping does not modify the standard way of deriving the luminosity and angular diameter distances and they both are calculated as follows,

$$\begin{aligned} D_L(z_{\text{obs}}) &= (1 + z_{\text{obs}}) D_H f_C[D_M(z_{\text{obs}})/D_H] \\ D_A(z_{\text{obs}}) &= \frac{1}{1 + z_{\text{obs}}} D_H f_C[D_M(z_{\text{obs}})/D_H], \end{aligned} \quad (11)$$

where  $D_H = (c/H_0)/\sqrt{|\Omega_k|}$  and

$$f_C(x) = \begin{cases} \sinh(x) & \Omega_k > 0, \\ x & \Omega_k = 0, \\ \sin(x) & \Omega_k < 0. \end{cases} \quad (12)$$

It is easy to check that both distances conform to the postulated distance-duality relation given by 9.  $D_L$  and  $D_A$  are measured from Type Ia supernova and BAO data, respectively.

#### 3.2 Hubble parameter

The local determination of the Hubble constant and the measurements of the Hubble parameter from BAO observations rely in general on the same key idea of measuring the ratio of the redshift (velocity) intervals to the corresponding distance scales. Measurements of distances make use of various external distance calibrators such as cepheids (for the local measurements) or the BAO scale from the CMB (for the BAO-based measurements). Therefore, they are obviously independent of redshift remapping. It is then easy to notice that redshift remapping modifies the measured Hubble parameter only through the observed redshift interval  $dz_{\text{obs}}$ , i.e.  $H_{\text{obs}}(z_{\text{obs}}) \sim dz_{\text{obs}}$ .

In the framework built upon redshift remapping, the observationally determined Hubble parameter is no longer identical to the Hubble parameter in the Friedmann equation. Hereafter, we shall refer the former as  $H_{\text{obs}}(z_{\text{obs}})$  and to the latter as  $H(z_{\text{FLRW}})$ . The relation between both of them can be easily found by transforming the observed redshift interval  $dz_{\text{obs}}$  into the corresponding interval  $dz_{\text{FLRW}}$ :

$$H_{\text{obs}}(z_{\text{obs}}) = \frac{H[z_{\text{FLRW}}(z_{\text{obs}})]}{dz_{\text{FLRW}}/dz_{\text{obs}}} = \frac{H[z_{\text{obs}}(1 + \alpha)]}{1 + \alpha + z_{\text{obs}}d\alpha/dz_{\text{obs}}}. \quad (13)$$

As a special case of the above equation, we can see that redshift remapping implies that the locally measured Hubble constant,

$$H_{\text{obs } 0} = H_{\text{obs}}(z_{\text{obs}} = 0) = h_{\text{obs}} 100 \text{ km s}^{-1} \text{ Mpc}^{-1}, \quad (14)$$

cannot be identified with the actual Hubble constant,

$$H_0 = H(z_{\text{obs}} = 0) = h 100 \text{ km s}^{-1} \text{ Mpc}^{-1}, \quad (15)$$

related to the global expansion of space. Using  $z_{\text{obs}} = 0$  we find that

$$H_{\text{obs } 0} = \frac{H_0}{1 + \alpha(0)}. \quad (16)$$

With the adopted priors on redshift remapping motivated by cosmological fits with dark-matter-dominated models, we expect  $H_{\text{obs } 0} \leq H_0$ .

Some measurements of the BAO signal constrain the volume averaged distance combining the observed Hubble parameter and the angular diameter distance. This distance is given by the following formula

$$D_V(z_{\text{obs}}) = \left( \frac{D_A^2(z_{\text{obs}})}{cH_{\text{obs}}(z_{\text{obs}})} \right)^{1/3}. \quad (17)$$

Dependence on redshift remapping occurs via equations (11) and (13).

The Hubble parameter can be estimated from observations of cosmic chronometers which are pairs of passively evolving galaxies separated in redshift space by a small range  $dz_{\text{obs}}$  (Jimenez & Loeb 2002). Passive evolution of both galaxies allows for estimating the corresponding cosmic time interval  $dt$  as a difference between stellar ages of the two galaxies. The resulting ratio of the redshift-to-time interval constrains the expansion rate via the following equation:

$$H_{\text{CC}}(z_{\text{obs}}) = -\frac{1}{1+z_{\text{obs}}} \frac{dz_{\text{obs}}}{dt}. \quad (18)$$

The above observable equals to the Hubble parameter  $H(z_{\text{obs}})$  given by the Friedmann equation when the standard mapping between  $z_{\text{obs}}$  and the scale factor is assumed, i.e. ( $z_{\text{FLRW}} = z_{\text{obs}}$ ). Redshift remapping, however, leads to the following modification:

$$H_{\text{CC}}(z_{\text{obs}}) = \frac{H[z_{\text{FLRW}}(z_{\text{obs}})]}{1+z_{\text{obs}}} \frac{1+z_{\text{FLRW}}}{1+\alpha+z_{\text{obs}}d\alpha/dz_{\text{obs}}}. \quad (19)$$

### 3.3 Cosmic Microwave Background

We begin our considerations with a general statement that redshift evolution of the CMB temperature can be derived without any assumption about the mapping between the cosmological redshift and cosmic scale factor, and thus it does not depend on redshift remapping. In fact, the standard relation between the CMB temperature and the observed redshift, i.e.  $T \sim (1+z_{\text{obs}})$ , and the conservation of the blackbody spectrum are equivalent to the distance-duality relation (Räsänen et al. 2016). Since the distance-duality relation holds in our model, the standard dependence of the CMB temperature on  $z_{\text{obs}}$  as well as the blackness of the CMB spectrum, the former confirmed by observations of the Sunyaev-Zel'dovich effect (Saro et al. 2014; Luzzi et al. 2015) and the latter tested in the measurements of the spectral energy distribution of the CMB (Ellis et al. 2013; Fixsen et al. 1996), remain unchanged, no matter what mapping between  $z_{\text{obs}}$  and cosmic scale factor  $a$  is adopted.

The present temperature of the CMB fixes the redshift of recombination at  $z_{\text{obs rec}} \approx 1100$ . Finding the scale factor at the epoch of recombination requires going beyond the observational basis and assuming a mapping between  $z_{\text{obs}}$  and the corresponding scale factor. In contrast to the standard cosmological framework in which  $a = 1/(1+z_{\text{obs}})$ , this scale factor is effectively a free parameter in our model (an unconstrained value of redshift remapping at the redshift of recombination). Therefore, the main effect of redshift remapping on the CMB modeling is to change the scale factor of recombination from  $a_{\text{rec}} = 1/(1+z_{\text{obs rec}})$  to

$$a_{\text{rec}} \equiv \frac{1}{1+z_{\text{FLRW rec}}} = \frac{1}{1+z_{\text{obs rec}}[1+\alpha(z_{\text{obs rec}})]}. \quad (20)$$

We use the *camb* code (Lewis et al. 2000) to compute the CMB temperature (TT) power spectrum. The standard mapping between the scale factor and the cosmological redshift is a built-in relation in the code which is used to determine the scale factor of recombination given the measured temperature of the CMB  $T_{\text{obs } 0}$ . An easy way to incorporate redshift remapping into the framework of the code is to replace the input CMB temperature in *camb* by an auxiliary temperature  $T_0$  given by

$$T_0 = T_{\text{obs } 0} \frac{1+z_{\text{obs rec}}}{1+z_{\text{FLRW rec}}} \approx T_{\text{obs } 0} \frac{1}{1+\alpha(z_{\text{obs rec}})}. \quad (21)$$

The auxiliary temperature is effectively a free parameter which sets the scale factor of recombination based on the standard  $a - z_{\text{rec}}$  mapping, i.e.

$$a_{\text{rec}} = \frac{T_0}{T_{\text{rec}}}, \quad (22)$$

where  $T_{\text{rec}}$  is the CMB temperature at the epoch of recombination. The power spectrum calculated for the auxiliary temperature does not describe the actual measurements of the CMB temperature anisotropies. It merely represents the power spectrum of a model with the standard redshift mapping and the current CMB temperature equal to the auxiliary temperature  $T_0$ . In order to make it represent the actual CMB observations, it has to be transformed according to the conversion of the CMB temperature from the auxiliary temperature  $T_0$  back to the observed temperature  $T_{\text{obs } 0}$ . This transformation involves both scaling the CMB temperature fluctuation  $\Delta T$  and the angular diameter distance  $D_A$  to the last scattering surface in the following way:

$$\begin{aligned} \Delta T &\rightarrow \Delta T(T_{\text{obs } 0}/T_0) \\ D_A &\rightarrow D_A \frac{1+z_{\text{FLRW rec}}}{1+z_{\text{obs rec}}} = D_A(T_{\text{obs } 0}/T_0). \end{aligned} \quad (23)$$

The latter scaling stems directly from the distance-duality relation in which the conversion from the auxiliary to the actual CMB temperature results in replacing the factor  $(1+z_{\text{FLRW}})$  by  $(1+z_{\text{obs}}) = (1+z_{\text{FLRW}})(T_0/T_{\text{obs } 0})$ . Using the above conversions of angular diameter distance and the CMB temperature we find that the power spectrum  $C_l$  and the multipole numbers transform in the following way:

$$\begin{aligned} C_l &\rightarrow C_l(T_{\text{obs } 0}/T_0)^2 \\ l &\rightarrow l(T_{\text{obs } 0}/T_0) \end{aligned} \quad (24)$$

The whole transformation is independent of the order of these two scaling relations given above. The transformation of the multipole numbers assumes the approximation of small angles. Therefore, we limit our analysis of the CMB temperature power spectrum to high multipoles with  $l \geq 30$ .

The procedure outlined above becomes very intuitive in a plausible scenario in which redshift remapping is related to a physical effect operating at late times of cosmic evolution, i.e. the epoch of non-linear structure formation. In this case, a non-vanishing  $\alpha(z_{\text{obs rec}})$  is simply a residual effect of the propagation of the CMB photons at late times. Thus, this effect does not coincide with the physics of the

early universe determining the CMB properties and it can be separated from the model by applying well-defined transformations of the CMB temperature and the angular scales of the CMB temperature anisotropies. It is not guaranteed, however, that cosmological fits with redshift remapping do not require some modifications of the CMB lensing. In order to keep the model as general as possible, we treat the lensing amplitude in *camb* as a free parameter (see below).

#### 4 DATA SETS AND METHODS

We distinguish two main groups of cosmological data sets: low-redshift probes (LZ) and high-redshifts probe (HZ). The former constrains redshift remapping at redshifts  $z_{\text{obs}}$  between 0 and 2.5 and includes observations of Type Ia supernovae, BAO, cosmic chronometers and the local measurement of the Hubble constant. The latter places constraints on redshift remapping at the redshift of recombination and includes the power spectrum of the CMB temperature anisotropies.

In the LZ data set, we use apparent magnitudes of Type Ia supernovae resulting from a joint likelihood analysis (JLA) of SDSS-II and SNLS supernova samples (Betoule et al. 2014). The data set consists of supernova magnitudes averaged in 31 redshift bins and the associated covariance matrix. Second, we use a compilation of BAO measurements combining results from four spectroscopic surveys: SDSS-III/BOSS (Alam et al. 2015), WiggleZ (Parkinson et al. 2012), SDSS-MGS (Abazajian et al. 2009) and 6dF (Jones et al. 2009). The BOSS data set includes constraints on the Hubble parameter and angular diameter distance inferred from galaxy clustering in three redshift bins centered at  $z_{\text{obs}} = 0.38, 0.51, 0.61$ , flux-correlation of the Ly- $\alpha$  forest of BOSS quasars at effective redshift  $z_{\text{obs}} = 2.34$  (Delubac et al. 2015) and from the cross-correlation of quasars with the Ly- $\alpha$  forest at effective redshift  $z_{\text{obs}} = 2.36$  (Font-Ribera et al. 2014). For the three low redshift bins, we use the consensus best-fit values and the covariance matrix obtained by combining results of four independent pre-reconstruction methods of measuring the BAO signal (Alam et al. 2016). The two BAO measurements at high redshifts are practically uncorrelated (Delubac et al. 2015) and therefore both are described by two independent covariance matrices. Since  $H_{\text{obs}}$  is only mildly anticorrelated with  $D_A$  in both cases, we use diagonal covariance matrices. The WiggleZ data provides the measurements of the volume-averaged distance  $D_V$  in three redshift bins at effective redshifts  $z_{\text{obs}} = 0.44, 0.60, 0.73$  (Kazin et al. 2014). Our analysis takes into account the full covariance matrix quantifying correlations arising from partial overlaps between redshift bins. Finally, we also make use of single measurements of  $D_V$  from the 6dF survey at effective redshift  $z_{\text{obs}} = 0.106$  (Beutler et al. 2011) and from the Main Galaxy Sample of the SDSS (SDSS-MGS) at effective redshift  $z_{\text{obs}} = 0.15$  (Ross et al. 2015). All BAO measurements used in this work are summarized in Table 1 and shown in Fig. 4. They are consistently rescaled to the same value of the sound horizon  $r_{s \text{ fid}} = 147.78$  Mpc assumed in (Alam et al. 2016) for a fiducial flat  $\Lambda$ CDM cosmological model with  $\Omega_m = 0.31$ , baryon density  $\Omega_b h^2 = 0.022$ , Hubble constant  $h = 0.676$ , fluctuation amplitude  $\sigma_8 = 0.83$ , spectral tilt  $n_s = 0.97$

and the reionization optical depth  $\tau = 0.078$ . The fiducial cosmological parameters are within  $1\sigma$  range of the best-fit Planck2015 values (Planck Collaboration et al. 2016b). Without loss of generality, we hereafter refer to the fiducial model as the Planck cosmological model.

The LZ data set is complemented by the local measurement of the Hubble constant from (Riess et al. 2016), i.e.  $H_{\text{obs } 0} = (73.24 \pm 1.74) \text{ km s}^{-1} \text{ Mpc}^{-1}$ . Including this measurement in our analysis allows us to place constraints on  $r_s$  independently of CMB observations. Finally, we also include the estimates of the Hubble parameter  $H_{\text{CC}}$  from observations of cosmic chronometers (see Table 2).

The HZ data set includes the temperature power spectrum from the Planck 2015 data release (Planck Collaboration et al. 2016a). We compute the likelihood function using the standard code provided as a part of the Planck Legacy Archive. Due to small-angle approximation assumed in equation (24), we restrict our analysis to high multipoles with  $l \geq 30$  available in a data set named *plik\_dx11dr2\_HM\_v18\_TT.clik*. The likelihood function depends on a theoretical power spectrum and 16 nuisance parameters describing the foreground sources. We use the recommended priors for the foreground parameters.

We use a Monte Carlo Markov Chain technique to find best-fitting models. The likelihood function for the LZ data set is given by  $\exp(-\chi^2/2)$ , where  $\chi^2$  function is computed using the covariance matrix whose blocks are given by covariance matrices of the subsequent data subsets.

#### 4.1 Parameters

The LZ data set constrains redshift remapping, the matter density parameter  $\Omega_m$ , the Hubble constant  $H_0$  and the sound horizon scale  $r_s$ . As outlined in section 2.1, redshift remapping is specified by 6 parameters with priors arising from fitting cosmological models without dark energy and reducing the allowed family solutions to monotonic functions (without distinct features). The matter density parameter is a free parameter for fits with open cosmological models and it is fixed at  $\Omega_m = 1$  for flat models. Normalization of the Hubble diagram of Type Ia supernovae is an additional nuisance parameter.

Theoretical TT power spectra in our model depends on 8 parameters (or 7 parameters assuming flat models), i.e. the cold dark matter density parameter  $\Omega_c$ , the baryonic matter density parameter  $\Omega_b$ , the Hubble constant  $h$ , the scalar spectral index  $n_s$ , normalization of the power spectrum given by  $\sigma_8$ , reionization optical depth  $\tau$ , value of redshift remapping given by the ratio  $T_{0 \text{ obs}}/T_0$  and parameter  $A_L$  scaling the standard lensing potential power spectrum (Calabrese et al. 2008). We assume the same neutrino sector as in a Planck baseline  $\Lambda$ CDM cosmological model (Planck Collaboration et al. 2016b), i.e. the effective number of neutrinos  $N_{\text{eff}} = 3.046$  and a single massive eigenstate with the corresponding density parameter  $\Omega_\nu h^2 = 0.0006$ . We adopt  $T_{0 \text{ obs}} = 2.7255$  K as our fiducial value of the measured CMB temperature (Fixsen 2009). Finally, we use a default value of the mass fraction in Helium assumed in standard Planck cosmological fits, i.e.  $Y_p = 0.2477$ .



$z_{\text{obs}}$	observable	measurement	survey	reference
0.106	$D_V$ [Mpc]	439	6dF	(Beutler et al. 2011)
0.15	$D_V$ [Mpc]	660	MGs	(Ross et al. 2015)
0.38	$D_M$ [Mpc]	1529	BOSS	(Alam et al. 2016)
0.38	$H_{\text{obs}}$ [km/s/Mpc]	81.2	BOSS	(Alam et al. 2016)
0.44	$D_V$ [Mpc]	1707	WiggleZ	(Kazin et al. 2014)
0.51	$D_M$ [Mpc]	2007	BOSS	(Alam et al. 2016)
0.51	$H_{\text{obs}}$ [km/s/Mpc]	88	BOSS	(Alam et al. 2016)
0.60	$D_V$ [Mpc]	2209	WiggleZ	(Kazin et al. 2014)
0.61	$D_M$ [Mpc]	2274	BOSS	(Alam et al. 2016)
0.61	$H_{\text{obs}}$ [km/s/Mpc]	96	BOSS	(Alam et al. 2016)
0.73	$D_V$ [Mpc]	2502	WiggleZ	(Kazin et al. 2014)
2.34	$D_A$ [Mpc]	1666	BOSS(Ly- $\alpha$ )	(Delubac et al. 2015)
2.34	$H_{\text{obs}}$ [km/s/Mpc]	221	BOSS(Ly- $\alpha$ )	(Delubac et al. 2015)
2.36	$D_A$ [Mpc]	1593	BOSS(Ly- $\alpha$ )	(Font-Ribera et al. 2014)
2.36	$H_{\text{obs}}$ [km/s/Mpc]	225	BOSS(Ly- $\alpha$ )	(Font-Ribera et al. 2014)

**Table 1.** BAO measurements (best-fit values) used in this work. All results are calibrated with the same fiducial value of the sound horizon  $r_s = 147.78$  Mpc.

$z_{\text{obs}}$	$H_{CC}$ [km s $^{-1}$ Mpc $^{-1}$ ]	reference
0.1	$69 \pm 12$	(Simon et al. 2005)
0.17	$83 \pm 8$	(Simon et al. 2005)
0.1791	$75 \pm 4$	(Moresco et al. 2012)
0.1993	$75 \pm 5$	(Moresco et al. 2012)
0.27	$77 \pm 14$	(Simon et al. 2005)
0.3519	$83 \pm 14$	(Moresco et al. 2012)
0.4	$95 \pm 17$	(Simon et al. 2005)
0.48	$97 \pm 60$	(Stern et al. 2010)
0.5929	$104 \pm 13$	(Moresco et al. 2012)
0.6797	$92 \pm 8$	(Moresco et al. 2012)
0.7812	$105 \pm 12$	(Moresco et al. 2012)
0.8754	$125 \pm 17$	(Moresco et al. 2012)
0.88	$90 \pm 40$	(Stern et al. 2010)
0.9	$117 \pm 23$	(Simon et al. 2005)
1.037	$154 \pm 20$	(Moresco et al. 2012)
1.3	$168 \pm 17$	(Simon et al. 2005)
1.363	$160 \pm 33.6$	(Moresco 2015)
1.43	$177 \pm 18$	(Simon et al. 2005)
1.53	$140 \pm 14$	(Simon et al. 2005)
1.75	$202 \pm 40$	(Simon et al. 2005)
1.965	$186.5 \pm 50.4$	(Moresco 2015)

**Table 2.** Measurements of the Hubble parameter  $H_{CC}$  from observations of cosmic chronometers.

## 5 RESULTS

In this section we summarize results of fitting dark-matter-dominated cosmological models with redshift remapping. We consider two background cosmological models: open cold-dark-matter-dominated models (oCDM $\alpha$ ) and a flat model with  $\Omega_m = 1$  (the Einstein-deSitter model, hereafter EdS $\alpha$ ). The models are constrained by the two data sets described in the previous section: low-redshift (LZ) data set including Type Ia supernovae, BAO, cosmic chronometers and the local determination of the Hubble constant; and high-redshift (HZ) data set including the CMB temperature power spectrum from the Planck observations (high multipoles). We present constraints from both data sets analyzed

separately and in a joint analysis combining both of them (LZ+HZ). We also consider a cosmological fit for a subset of the LZ data set which excludes the cosmic chronometer data (LZ-CC).

### 5.1 Open model (oCDM $\alpha$ )

Fig. 2 shows constraints on three parameters in common to modeling both LZ and HZ data sets: the matter density parameter  $\Omega_m$ , the sound horizon scale  $r_s$  and the Hubble constant  $h$ . The plots serve as an important test of consistency between both data sets. A remarkable agreement between constraints from the LZ and HZ data sets demonstrates that redshift remapping lays a self-consistent framework for a joint analysis of the CMB and low-redshift probes. The new framework yields consistency between the CMB and low-redshift data in terms of constraints on the Hubble constant and the sound horizon scale. As recently shown in (Bernal et al. 2016), the standard cosmological framework based on a  $\Lambda$ CDM cosmological model and the standard  $a - z_{\text{obs}}$  fails to pass this consistency test unless the cosmological constant is replaced by a phantom-like dark energy (Di Valentino et al. 2016).

Both LZ and HZ data sets favor nearly flat cosmological models with a low value of the Hubble constant. The matter density parameter from the LZ data set is strongly degenerated with the Hubble constant along the line of constant age of the Universe. As shown in Fig. 2, the 68% contour lies between the isochrone lines of 13 Gyr and 14 Gyr. The corresponding degeneracy line of constraints from the HZ data set is substantially steeper than curves of constant age. The age of 14 Gyr corresponds to  $\Omega_m \approx 0.9$  and flatness necessitates the age larger than 15 Gyr.

Table 3 lists constraints on all parameters. Three columns show the results from separate analyses of the two data sets (LZ, HZ) and from a joint analysis combining both of them (LZ+HZ). Compared to the Planck cosmological model, the scalar spectral index  $n_s$  and the deionization optical depth  $\tau$  remain unchanged, whereas  $\sigma_8$  is 7% smaller. Constraints on all remaining parameters un-

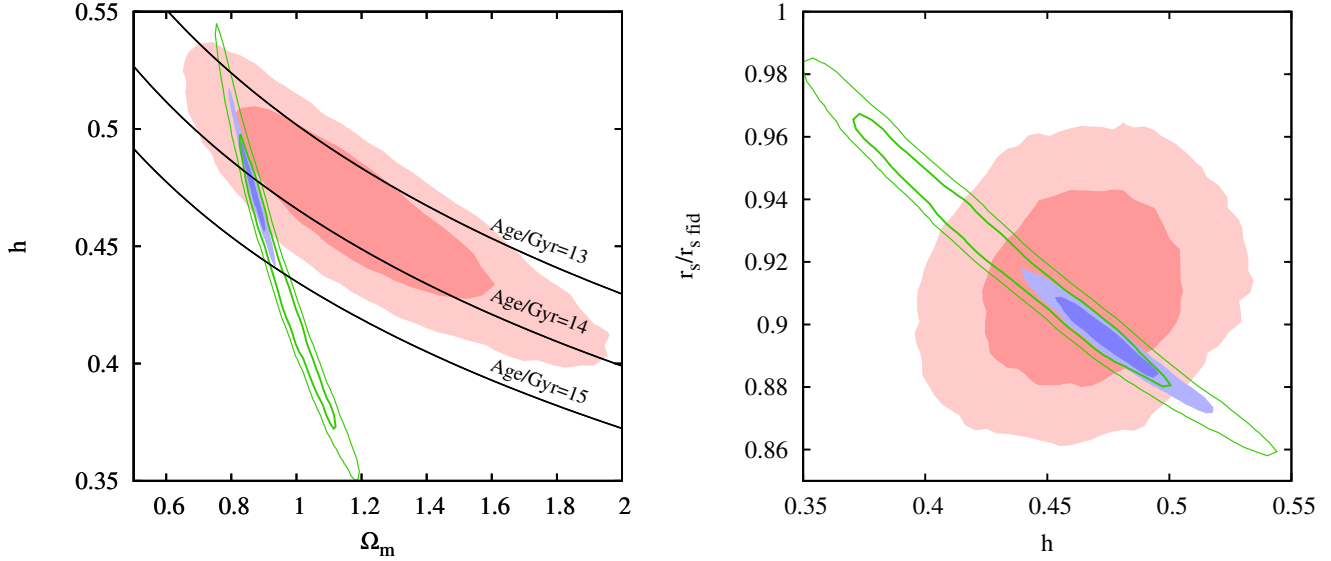


**Figure 2.** Marginalized 68% and 95% confidence level constraints on the matter density parameter  $\Omega_m$ , the Hubble constant  $h$  and the sound horizon scale  $r_s$  (relative to the fiducial value  $r_{s \text{ fid}} = 147.78$  Mpc for the Planck  $\Lambda$ CDM cosmology) assuming an open CDM cosmological model with redshift remapping (oCDM $\alpha$ ). The red and green contours show constraints from the LZ and HZ data sets, whereas the blue contours from a joint analysis combining both data sets. The black lines are curves of constant age of the Universe fixed at 13, 14 and 15 Gyr.

dergo significant modification. Dark-matter-dominated cosmological model with redshift remapping is characterized by higher density of baryons and cold dark matter, but nearly the same baryon-to-dark matter fraction as in Planck cosmology. The sound horizon scale is  $\sim 10\%$  smaller than its value in the standard  $\Lambda$ CDM model. A joint analysis of the LZ and HZ data sets yields a small curvature with  $\Omega_K = 1 - \Omega_m = 0.13 \pm 0.03$ . Finally, the new oCDM $\alpha$  model with redshift remapping requires suppression of smoothing of the power spectrum due to lensing based on the standard template of the lensing potential. The best-fit amplitude of the lensing potential is  $0.65 \pm 0.07$  (65% of the standard lensing amplitude).

Fig. 3 presents the key result of our work which is a non-parametric reconstruction of redshift remapping. The red contours and the red point at  $z_{\text{obs}} \approx 1100$  show constraints from separate analyses of the LZ and HZ data sets, whereas the blue from a joint analysis combining both data sets. Without loss of sufficient precision, when computing redshift remapping at the CMB redshift, we approximate  $(1 + z_{\text{FLRW}})/(1 + z_{\text{obs}}) = T_{0 \text{ obs}}/T_0$  (given in Table 3) by  $z_{\text{FLRW}}/z_{\text{obs}}$ . The green lines and arrows show redshift distribution (or redshift locations) of the different cosmological probes used in this work.

Although the adopted priors allow for a constant profile, redshift remapping clearly appears to be a function increasing with redshift. In particular, the difference between redshift remapping at the ends of the interpolation range, i.e.  $z_{\text{obs}} = 0$  and  $z_{\text{obs}} = 2.5$ , is  $0.21 \pm 0.05$  for LZ and  $0.11 \pm 0.02$  for LZ+HZ. It is also well visible from Fig. 3 that the bulk change of redshift remapping in the redshift range of the LZ data set occurs at  $z_{\text{obs}} \lesssim 0.8$ .

Results from independent analyses of the LZ and HZ data sets indicate that redshift remapping may exhibit a

plateau at  $z_{\text{obs}} \gtrsim 2.5$  extending up to the recombination redshift. This kind of plateau would be the simplest form of interpolation between the LZ data and the CMB, i.e. between  $z_{\text{obs}} \approx 2.5$  and  $z_{\text{obs}} \approx 1100$ . Results from the joint analysis suggest that redshift remapping should continue to increase at  $z_{\text{obs}} > 2.5$  in order to match the value determined from the CMB. This, however, does not rule out the presence of a plateau at higher redshift. Assuming a naive linear extrapolation of redshift profile determined from the LZ data set, we can see that redshift remapping may reach its value from the CMB at  $z_{\text{obs}} \approx 10$ .

Redshift remapping reconstructed from the LZ data is fully consistent with constraints from the joint analysis. Adding the HZ data results only in a small reduction of the remapping at  $z_{\text{obs}} > 1$ . The remaining part of the profile remains nearly unchanged (despite a two fold increase of the reconstruction precision).

The confidence intervals of the reconstructed redshift remapping clearly demonstrate that the data constrain the remapping values below 1 at all redshifts. This means that the scale factor assigned to the observed redshift  $z_{\text{obs}}$  in the reconstructed redshift remapping is always larger than that obtained from the standard relation  $1 + z_{\text{obs}} = 1/a$ . From the purely data-based point of view, the deviation of the reconstructed redshift remapping from the standard  $1 + z_{\text{obs}} = 1/a$  relation corresponds a positive cosmological constant in a  $\Lambda$ CDM cosmological model with the standard mapping between the cosmological redshift and cosmic scale factor. Adding a cosmological constant in our background model would result in a strong degeneracy between the expansion history and redshift remapping with a one-to-one correspondence between consecutive values of the cosmological constant and gradually flattening profiles of redshift remapping, as shown in (Wojtak & Prada 2016).

parameter	HZ	LZ	LZ+HZ
$100\Omega_b h^2$	$2.90 \pm 0.28$	-	$3.12 \pm 0.13$
$\Omega_c h^2$	$0.152 \pm 0.014$	-	$0.163 \pm 0.005$
$h$	$0.439 \pm 0.042$	$0.464 \pm 0.027$	$0.475 \pm 0.016$
$n_s$	$0.969 \pm 0.008$	-	$0.968 \pm 0.008$
$\tau$	$0.106 \pm 0.050$	-	$0.086 \pm 0.045$
$\sigma_8$	$0.772 \pm 0.034$	-	$0.774 \pm 0.035$
$T_{\text{obs } 0}/T_0$	$0.920 \pm 0.028$	-	$0.896 \pm 0.010$
$A_L$	$0.638 \pm 0.070$	-	$0.650 \pm 0.068$
$1 + \alpha(0.0)$	-	$0.63 \pm 0.05$	$0.64 \pm 0.02$
$1 + \alpha(0.5)$	-	$0.71 \pm 0.04$	$0.69 \pm 0.02$
$1 + \alpha(1.0)$	-	$0.75 \pm 0.05$	$0.71 \pm 0.02$
$1 + \alpha(2.5)$	-	$0.84 \pm 0.07$	$0.75 \pm 0.03$
$d\alpha/dz_{\text{obs}}(0.0)$	-	$0.141 \pm 0.076$	$0.115 \pm 0.065$
$d\alpha/dz_{\text{obs}}(2.5)$	-	$0.082 \pm 0.015$	$0.044 \pm 0.012$
$\Omega_m$	$0.953 \pm 0.098$	$1.21 \pm 0.27$	$0.868 \pm 0.031$
$r_s/\text{Mpc}$	$135.9 \pm 4.1$	$134.8 \pm 3.1$	$132.4 \pm 1.4$
Age/Gyr	$15.13 \pm 1.15$	$13.59 \pm 0.41$	$14.13 \pm 0.37$

**Table 3.** Posterior mean and standard deviation for the parameters of an open CDM model with redshift remapping ( $\text{oCDM}\alpha$ ). The left column shows constraints from the HZ data set (Planck CMB temperature power spectrum), the middle column from the LZ data set (SN Ia, BAO,  $H_0$  and cosmic chronometers) and the right column from a joint analysis combining both data sets. The top part of the table contains all relevant parameter for calculating the CMB temperature power spectrum, the middle part lists constraints on the parameters of redshift remapping at the interpolation knots and the bottom part shows selected derived parameters from the CMB analysis.

In summary, open CDM models with redshift remapping provide excellent fits to all data. Fig. 4 compares all cosmological measurements in the LZ data set to our best-fitting models and the fiducial flat  $\Lambda$ CDM cosmological model with Planck parameters (and the standard relation between the cosmological redshift and cosmic scale factor). Since the comparison of the Hubble parameter from BAO observations involves recalibration due to the new value of the sound horizon scale, we include the local measurement of the Hubble constant in the panel showing the data of cosmic chronometers. We also combine all constraints on distances from BAO observation in a single panel. The solid and dashed lines differentiate between the comoving distance  $D_M$  and the volume averaged distance  $D_V$ .

Our best-fitting models outperform the Planck  $\Lambda$ CDM cosmological model (with the standard  $a - z_{\text{obs}}$  mapping) in two respects. First, they alleviate a tension between Planck observations and the BAO measurements from the Ly- $\alpha$  forest of high redshift quasars. The improvement is particularly well visible for the Hubble parameter. The supposed persistence of this tension reported in our previous work (Wojtak & Prada 2016) turns out to be a result of assuming a fixed shape of redshift remapping. Second, redshift remapping also eliminates a discrepancy between the local measurement of the Hubble constant and its counterpart inferred from Planck data under the assumption of a flat  $\Lambda$ CDM cosmology (see the inset panel for the cosmic chronometer data).

Equally well goodness of fit is achieved for the CMB temperature power spectrum. Fig. 5 compares the Planck

power spectrum to our best-fitting open cosmological model with redshift remapping constrained by the HZ data set alone and the Planck  $\Lambda$ CDM cosmology. Due to small angle approximation, our fit makes use only of high multipole part of the power spectrum with  $l \geq 30$ . Therefore, its extrapolation to small multipoles (the blue dashed line) may be insufficiently accurate for a detailed comparison to the corresponding  $\Lambda$ CDM power spectrum.

The best-fitting power spectrum of an open model with redshift remapping is essentially indistinguishable from its  $\Lambda$ CDM counterpart. The maximum likelihood value is  $-379.8$  compared to  $-380.7$  for the Planck flat  $\Lambda$ CDM model with the standard mapping between the cosmological redshift and cosmic scale factor ( $T_0 = T_{0 \text{ obs}}$ ).

## 5.2 Flat model (EdS $\alpha$ )

As shown in Fig. 2, both LZ and HZ data sets, when analyzed separately, are fully consistent with a flat CDM model. It is therefore instructive to scrutinize whether or under what conditions the Einstein-deSitter model with redshift remapping can provide a satisfactory description of the two combined data sets. The major difficulty arises here from the fact the the CMB data constrain the Hubble constant to significantly smaller values than the LZ data set when assuming a flat model. This is well visible both in Fig. 2 and Fig. 6 which shows the marginalized constraints on the Hubble constant and the sound horizon scale for an EdS model with redshift remapping. The latter also proves that the problem of a tension between high and low redshift data

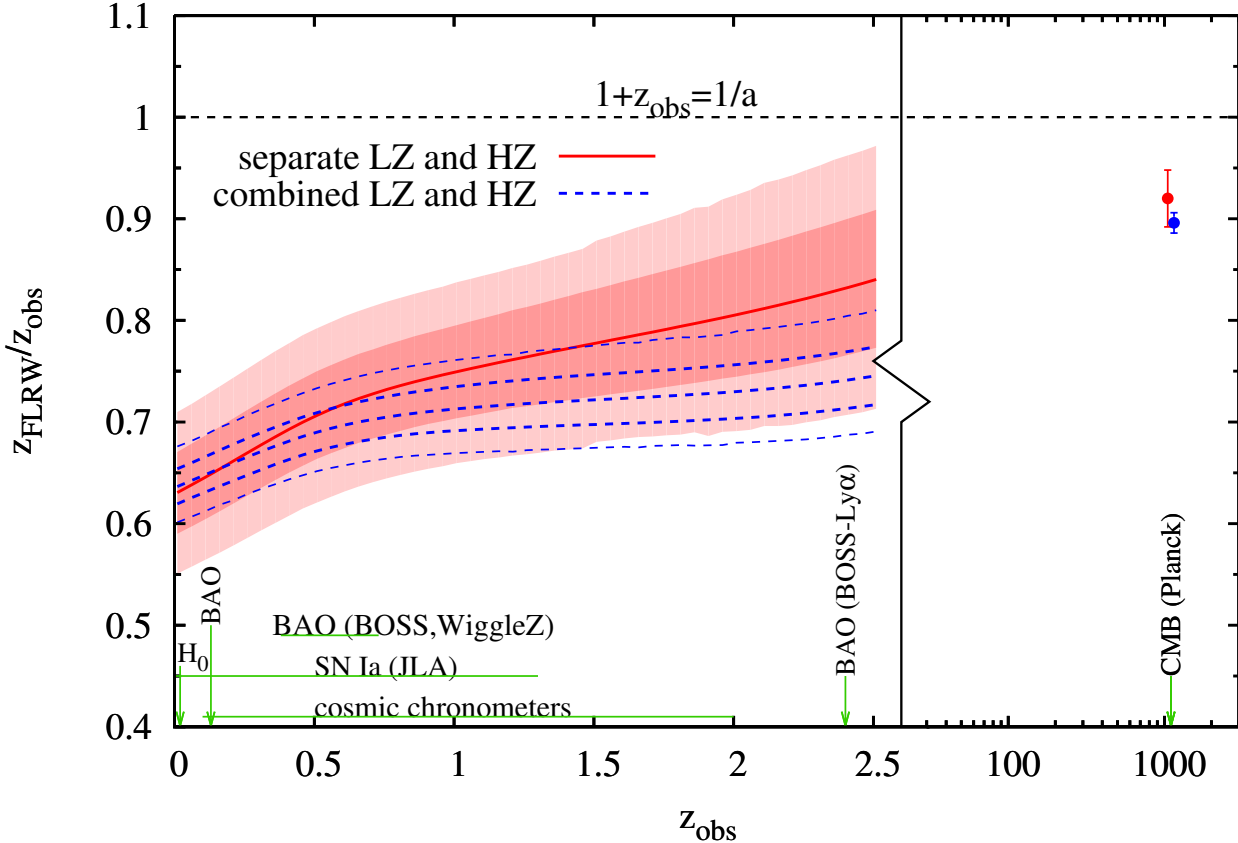


**Figure 3.** Non-parametric constraints on redshift remapping assuming open dark-matter-dominated cosmological models. The red and blue contours (data points at CMB redshift) show marginalized 68% and 95% confidence level constraints from a separate analysis of the LZ (SN Ia, BAO,  $H_0$  and cosmic chronometers) and HZ (Planck temperature power spectrum) data sets, and from a joint analysis combining the two data sets. The green lines and arrows show redshift distributions or redshift locations of different cosmological probes in the LZ data set ( $z_{\text{obs}} < 2.5$ ) and the HZ data set (CMB). The vertical lines marks the transition between a linear and logarithmic scale of  $z_{\text{obs}}$ .

does not concern the sound horizon scale: both the CMB and the LZ data provide fully consistent constraints on  $r_s$ .

Since the degeneracy between  $\Omega_m$  and  $h$  is much stronger for the CMB than for the LZ data (see Fig. 2), the assumption of flatness results in a much larger increase of the constraining power from the CMB than from low-redshift probes. The difference between constraining power of the two data sets is also reflected by the difference in size of the contours in Fig. 6. Bearing in mind the leading role of the CMB in a joint fit, we expect that the comparison between the LZ data and the best-fitting joint-fit model may reveal which fraction of the LZ data set is responsible for the tension between LZ and HZ data sets in terms of constraints on the Hubble constant  $h$ .

The best-fitting model (EdS $\alpha$ ) from a joint analysis combining the LZ and HZ data is shown in Fig. 4. The model exhibits an excellent agreement with all data points but the Hubble parameters from cosmic chronometers, in particular at high redshifts  $z_{\text{obs}} > 1$ . Reanalysis of the LZ set excluding the cosmic chronometer data confirms that cosmic chronometers are the main (and probably the only) source of the tension between the Hubble constant from the LZ and HZ data (see Fig. 6). Omitting the cosmic chronometer data seems to be the only way to combine constraints from the

LZ and HZ sets in a fully consistent way under the assumption of a flat cosmological model and this is how we proceed in the following part of this section. Without any attempt to justify our choice in a thorough way, we emphasize that the cosmic chronometer data set is the most affected by possible astrophysical biases among all cosmological probes compiled in the LZ data set. Keeping in mind the attractive simplicity of the EdS model and an appealing consistency with other LZ probes, we think that omitting the cosmic chronometer data is an acceptable tradeoff.

Table 4 summarizes constraints on all relevant parameters from separate analyses of the LZ-CC and HZ data sets, and from a joint analysis combining both data sets. The assumption of flatness does not change the constraints from the previous section for the following parameters:  $n_s$ ,  $\tau$ ,  $\sigma_8$  and  $A_L$ . Likewise an open model, the baryon-to-matter fraction is nearly the same as in the Planck  $\Lambda$ CDM cosmology. The main difference lies in substantially smaller value of the Hubble constant and larger age of the Universe, both measured down to a 0.5% precision in this case (5 fold increase with respect to fits with an open CDM model).

Fig. 7 shows constraints on redshift remapping for the Einstein-deSitter model. The remapping reconstructed from the LZ-CC data appears to resemble closely its  $\text{oCDM}\alpha$

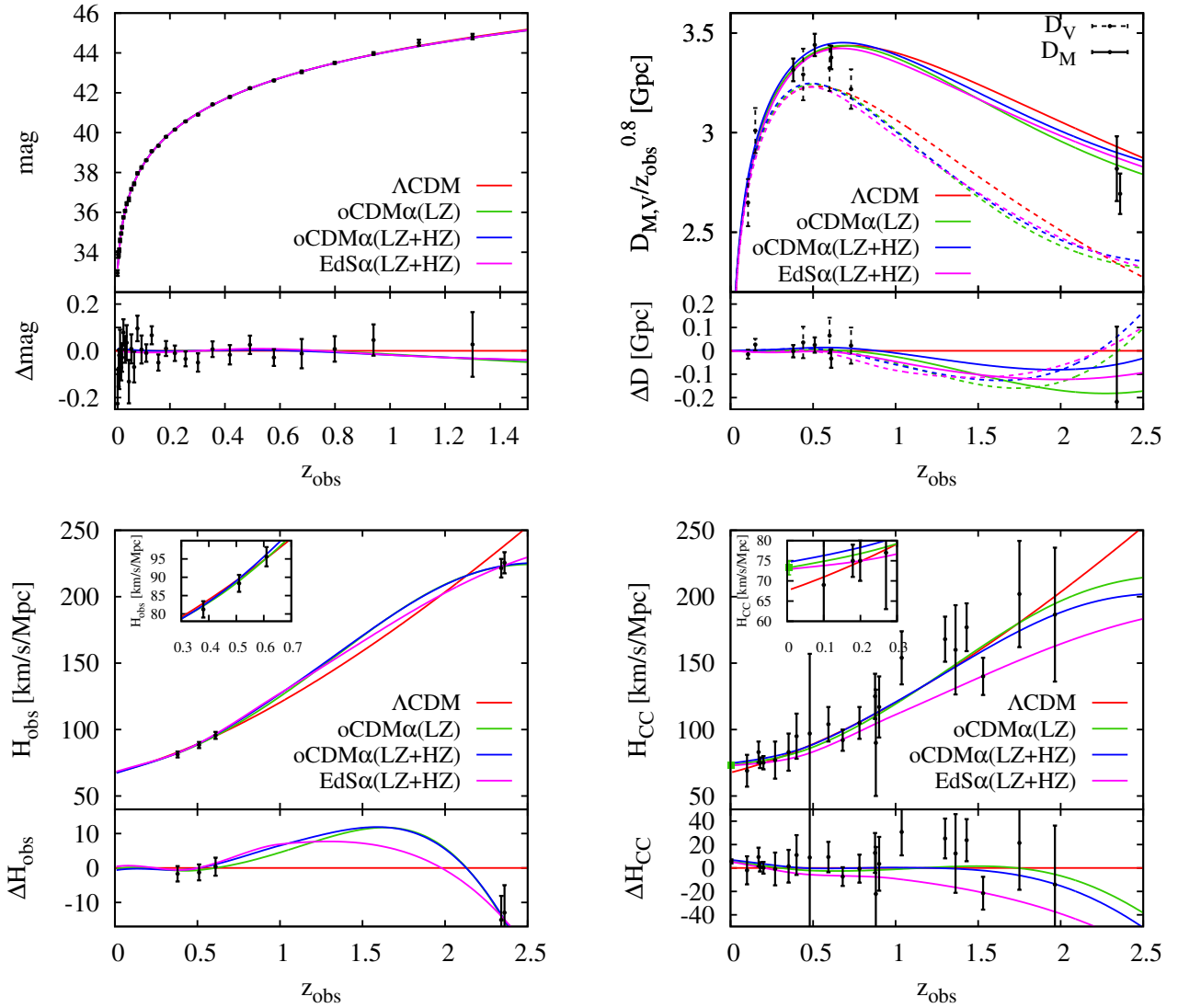


**Figure 4.** The LZ data used in this work compared to best-fitting cosmological models with redshift remapping and the Planck  $\Lambda$ CDM model. From top left clockwise, the panels show apparent magnitudes of Type Ia supernovae, distances from BAO observations (6dF, SDSS-MGS, WiggleZ, SDSS-III/BOSS), the Hubble parameter  $H_{CC}$  estimated from cosmic chronometers and the Hubble parameter  $H_{Obs}$  measured from BAO observations (BOSS). The local determination of the Hubble constant is shown in the bottom right panel. Best-fitting models include open CDM ( $\text{oCDM}\alpha$ ) and flat CDM (EdS $\alpha$ ) models with redshift remapping, constrained by the LZ data set alone (LZ) and by combined LZ and HZ data (LZ+HZ). The red curves show the predictions of the Planck flat  $\Lambda$ CDM cosmological model (with the standard mapping between the cosmological redshift and cosmic scale factor). All residuals are computed relative to the assumed Planck cosmological model.

counterpart shown in Fig. 3. The difference occurs when the CMB data are included in the analysis. In this case, the reconstructed redshift remapping appears to have noticeably smaller values than in the other reconstruction cases considered in this work. Its redshift profile follows closely the lower  $2\sigma$  envelope of the remapping reconstructed from the LZ data, regardless if the cosmic chronometer data are included in the fit or not. The overall slope, however, is similar to the remapping reconstructed from a joint analysis with an open cosmological model (see the blue contours in Fig. 3).

## 6 DISCUSSION AND CONCLUSIONS

We have demonstrated in this work that fitting dark-matter-dominated cosmological model with redshift remapping alters several properties and cosmological parameters which are well-established in the standard  $\Lambda$ CDM framework. In this section, we describe and summarize these modifications and explore possible consequences. We also enumerate several features of the new models which remain unchanged with respect to the Planck cosmology. We elaborate the importance of some of them in the context of sustaining consistency with other branches of cosmology such as Big Bang nucleosynthesis.

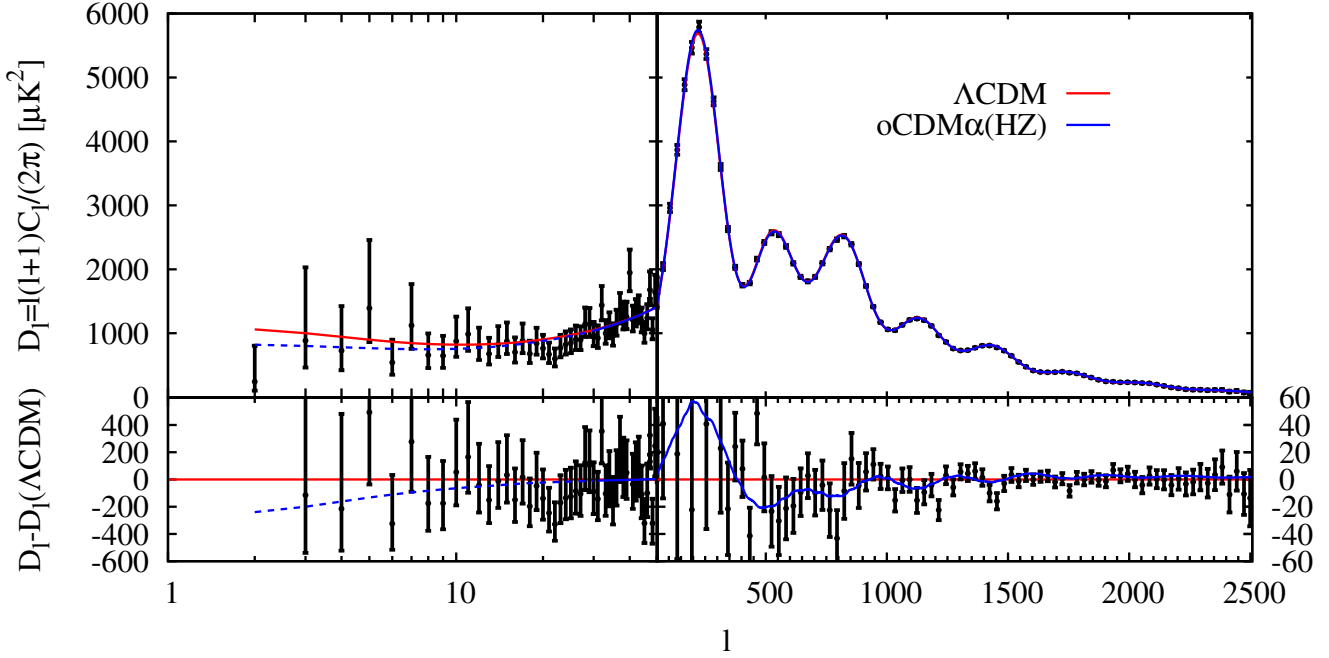


**Figure 5.** Planck CMB temperature power spectrum compared to the best-fitting open CDM model with redshift remapping (oCDM $\alpha$ , the blue line) and the Planck  $\Lambda$ CDM cosmology ( $\Lambda$ CDM, the red line). Due to small angle approximation, the best-fitting model is constrained by  $l \geq 30$  multipoles. Therefore, its extrapolation to small multipoles (the blue dashed line) may not be accurate enough for a detailed comparison to the corresponding  $\Lambda$ CDM model. The displayed Planck data consists of unbinned power spectrum at  $l < 50$  (linear scale on the plot) and binned measurements at  $l > 50$  (logarithmic scale on the plot). Residuals are computed relative to the assumed Planck cosmology. The black vertical lines separate a linear and logarithmic scale on the horizontal axis.

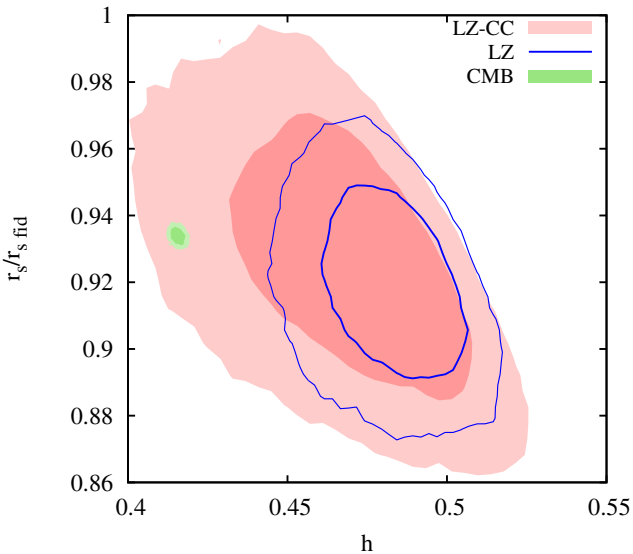


**Figure 6.** Marginalized 68% and 95% confidence level constraints on the Hubble constant  $h$  and the sound horizon scale  $r_s$  (relative to the fiducial value  $r_{s \text{ fid}} = 147.78$  Mpc for the Planck  $\Lambda$ CDM cosmology) assuming a flat CDM model (Einstein-deSitter) with redshift remapping (EdS $\alpha$ ). The blue and green contours show constraints from the LZ and HZ data sets, respectively. The red contours show results from an analysis of the LZ set omitting the cosmic chronometer data (LZ-CC).

## 6.1 Baryon content

The baryon fraction in our models is fully compatible with its analogous measurement within the standard  $\Lambda$ CDM framework. Our constraints on  $\Omega_b/\Omega_c$  are  $0.191 \pm 0.007$  for oCDM $\alpha$ (LZ+HZ) and  $0.189 \pm 0.006$  for EdS $\alpha$ (LZ-CC+HZ), compared to  $0.185 \pm 0.003$  derived from the Planck cosmological model. Consistency with the standard baryon fraction implies that the new models are not expected to introduce significant modifications to our current knowledge on the baryonic content in galaxy clusters. However, complete understanding of possible impact of the new models on the predicted properties of galaxy clusters will require carrying out hydrodynamical simulations with new cosmological parameters.

Another important aspect of the baryonic content in cosmological models is the baryon-to-photon number density ratio,  $\eta = n_b/n_\gamma$ . Redshift remapping modifies the ratio not only through a different baryon density parameter, but also through the fact that the number of photons is given by  $T_0^3$  rather than by  $T_{\text{obs}0}^3$  (since it is the former which is proportional to  $a^{-3}$ ). Combining these two effects leads to the following relation between the new ratio  $\eta$  and its value  $\eta_{\text{Planck}}$  in the Planck cosmological model with  $\Omega_b h^2 = 0.022$ :

$$\frac{\eta}{\eta_{\text{Planck}}} = \frac{\Omega_b h^2}{0.022} \left( \frac{T_{\text{obs}0}}{T_0} \right)^3. \quad (25)$$

Using best-fitting models established in a joint analysis of LZ and HZ data sets, we find  $\eta/\eta_{\text{Planck}} = 1.020 \pm 0.014$  for the oCDM $\alpha$  model and  $\eta/\eta_{\text{Planck}} = 1.016 \pm 0.013$  for the

parameter	HZ	LZ-CC	LZ-CC+HZ
$100\Omega_b h^2$	$2.730 \pm 0.057$	-	$2.730 \pm 0.057$
$\Omega_c h^2$	$0.1449 \pm 0.0017$	-	$0.1448 \pm 0.0017$
$h$	$0.416 \pm 0.002$	$0.466 \pm 0.026$	$0.416 \pm 0.002$
$n_s$	$0.966 \pm 0.008$	-	$0.967 \pm 0.008$
$\tau$	$0.099 \pm 0.051$	-	$0.100 \pm 0.049$
$\sigma_8$	$0.762 \pm 0.038$	-	$0.763 \pm 0.038$
$T_{\text{obs } 0}/T_0$	$0.936 \pm 0.004$	-	$0.935 \pm 0.004$
$A_L$	$0.642 \pm 0.072$	-	$0.643 \pm 0.073$
$1 + \alpha(0.0)$	-	$0.64 \pm 0.03$	$0.570 \pm 0.008$
$1 + \alpha(0.5)$	-	$0.71 \pm 0.04$	$0.617 \pm 0.007$
$1 + \alpha(1.0)$	-	$0.75 \pm 0.05$	$0.64 \pm 0.01$
$1 + \alpha(2.5)$	-	$0.83 \pm 0.08$	$0.67 \pm 0.02$
$d\alpha/dz_{\text{obs}}(0.0)$	-	$0.152 \pm 0.081$	$0.124 \pm 0.066$
$d\alpha/dz_{\text{obs}}(2.5)$	-	$0.067 \pm 0.023$	$0.024 \pm 0.010$
$\Omega_m$	1	1	1
$r_s/\text{Mpc}$	$138.0 \pm 0.45$	$137.0 \pm 4.0$	$138.0 \pm 0.38$
$\text{Age}/(10^9 \text{yrs})$	$15.68 \pm 0.07$	$14.0 \pm 0.8$	$15.68 \pm 0.07$

**Table 4.** Posterior mean and standard deviation for the parameters of a flat  $\Lambda$ CDM model ( $\Omega_m = 1$ ) with redshift remapping. The left column shows constraints from the HZ data set (Planck CMB temperature power spectrum), the middle columns from the HZ-CC data set (SN Ia, BAO and  $H_0$ , excluding cosmic chronometers) and the right column from a joint analysis combining both data sets. The top part of the table contains all relevant parameter for calculating the CMB temperature power spectrum, the middle part lists constraints on the parameters of redshift remapping at the interpolation knots and the bottom part shows selected derived parameters from the CMB analysis.

EdS $\alpha$  model. We obtain virtually no change in  $\eta$  compared to the Planck cosmology, what implies that our models preserve all standard prediction of the primordial nucleosynthesis. Needless to say, the assumed fraction of Helium in our analysis of the CMB power spectrum is fully consistent with the resulting baryon-to-photon number density ratio.

## 6.2 Hubble constant

The Hubble constant  $H_0$  in all models considered in this work appears to be much smaller than its locally observed value  $H_{\text{obs } 0}$ . The ratio of these two values of the Hubble constant is given by the local value of redshift remapping, as shown by equation 16, leading to

$$(H_{0 \text{ obs}} - H_0)/H_0 = \begin{cases} 0.60 \pm 0.10 & \text{(LZ)} \\ 0.575 \pm 0.046 & \text{(LZ+HZ)} \end{cases} \quad (26)$$

for the  $\Lambda$ CDM $\alpha$  model and

$$(H_{0 \text{ obs}} - H_0)/H_0 = \begin{cases} 0.57 \pm 0.08 & \text{(LZ-CC)} \\ 0.755 \pm 0.025 & \text{(LZ-CC+HZ)} \end{cases} \quad (27)$$

for the EdS $\alpha$  model.

The above relative differences between  $H_{0 \text{ obs}}$  and  $H_0$  coincide with the maximum expansion rates (relative to the Hubble constant  $H_0$ ) in voids formed in the corresponding cosmological models. Using our constraints on  $\Omega_m$ , approximating the maximum expansion rate by  $(3/2)\Omega_m^{0.6}$  (see (Bernardeau et al. 1997)) and taking its 1/3 contribution to redshift along the light paths, we find

$$\frac{1}{2}\Omega_m^{0.6} = \begin{cases} 0.56 \pm 0.07 & \text{(LZ)} \\ 0.46 \pm 0.01 & \text{(LZ+HZ)} \end{cases} \quad (28)$$

for the  $\Lambda$ CDM $\alpha$  model and 0.5 for the EdS $\alpha$  model. Apart from obvious disagreement for the EdS $\alpha$  model constrained by the LZ and HZ data sets, the maximum expansion rates are fairly consistent with the corresponding relative differences between the local and global values of the Hubble constant. This may be an incidental match, but it may also point to a role of voids in searching for the physical explanation of redshift remapping. The likelihood of the incident becomes even smaller if we realize that the new Hubble constant adjusts the age of the Universe in dark-matter-dominated models so that it is fully consistent with the current lower limits determined from observations of globular clusters (Gratton et al. 2003) and metal-poor stars (Bond et al. 2013).

The difference between  $H_0$  and  $H_{0 \text{ obs}}$  have several important consequences for the interpretation of the available observational data. In the following, we describe two interesting examples.

The very first argument for a low value of the total matter density parameter in the Universe was based on the measurement of the mass-to-light ratio in galaxy clusters. When combined with the mean luminosity density, it lead to  $\Omega_m \approx 0.2$  (see e.g. (Carlberg et al. 1997)). Correction of this estimate required by adopting models with redshift remapping can be deduced by considering basic scaling relations between the Hubble constant and different observables. On one hand, dynamical mass  $M \sim h_{\text{obs}}^{-1}$



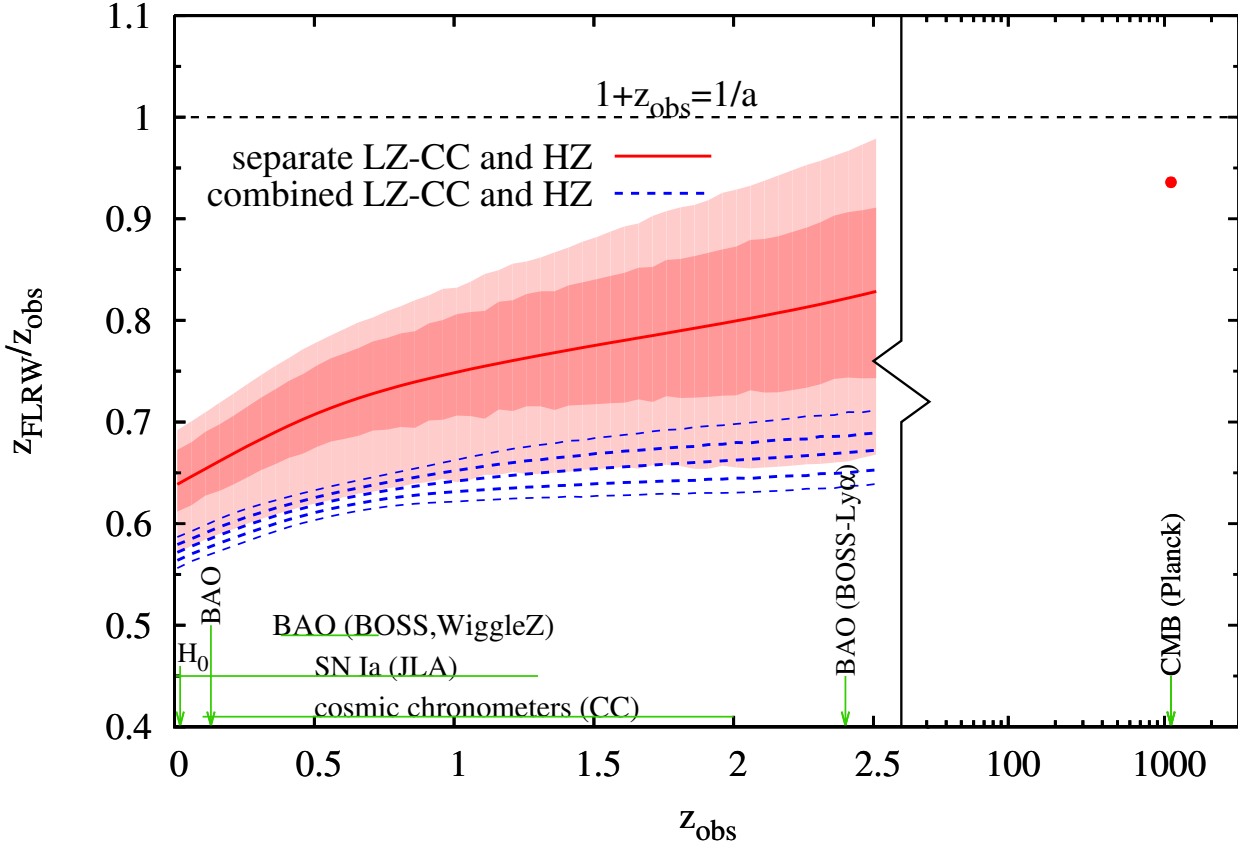


**Figure 7.** Non-parametric constraints on redshift remapping assuming a flat dark-matter-dominated cosmological model (the Einstein-deSitter model, EdS $\alpha$ ). The red and blue contours (and the data point at the redshift of recombination) show marginalized 68% and 95% confidence level constraints from a separate analysis of the LZ-CC (SN Ia, BAO and  $H_0$ , excluding cosmic chronometers) and HZ (Planck temperature power spectrum) data sets, and from a joint analysis combining both data sets. The green lines and arrows show redshift distributions or redshift locations of different cosmological probes in the LZ data set ( $z_{\text{obs}} < 2.5$ ) and the HZ data set (CMB). The vertical lines marks the transition between a linear and logarithmic scale of  $z_{\text{obs}}$ .

and luminosity  $L \sim h_{\text{obs}}^{-2}$  imply that the mass-to-light ratio ( $M/L$ )  $\sim h_{\text{obs}}$ . On the other hand, the luminosity density ( $L/V$ )  $\sim h_{\text{obs}}$  in the unit of the critical density  $\rho_c \sim h^2$  is ( $L/V/\rho_c$ )  $\sim h_{\text{obs}}/h^2$ . Combining these two relations leads to  $\Omega_m \sim (h_{\text{obs}}/h)^2$  and  $\Omega_m \approx (0.5 - 0.6)$  for our constraints on  $H_0$  obs/ $H_0$ . Therefore, the difference between the global and locally measured value of the Hubble constant predicted by our models implies the matter density parameter which is compatible with dark-matter-dominated cosmological model. Assuming the same bias of this measurement as in the standard  $\Lambda$ CDM model ( $\Omega_m \approx 0.2$  compared to  $\Omega_m = 0.31$  from Planck), we find  $\Omega_m \approx (0.8 - 0.9)$ , in agreement with constraints from analysis of LZ and HZ data.

The second example concerns the mass function. Having shown that constraints on the shape of the power spectrum are comparable to the  $\Lambda$ CDM case, we expect that the main effect modifying the mass function in our models stems from a higher value of the matter density parameter. Cosmological models with  $\Omega_m \approx 1$  predict in general higher density of dark matter haloes than observations. Comparing the mass functions of the EdS and  $\Lambda$ CDM model, we find that the former overestimates the abundance of haloes by  $\sim (0.5 - 0.6)$  dex (see (Jenkins et al. 2001)). Needless to say, this statement assumes implicitly equality between

$h$  and  $h_{\text{obs}}$  that is not true in the framework with redshift remapping. Correct comparison of the new mass function with observations requires applying conversion of the units from  $h^{-1}$  Mpc to  $h_{\text{obs}}^{-1}$  Mpc. This conversion lowers the mass function by  $3 \log_{10}(h_{\text{obs}}/h) \approx (0.6 - 0.7)$  what happens to compensate in large part the effect of large value of  $\Omega_m$ . Although any conclusion that the mass function in our models can be reconciled with the observed abundance of galaxy clusters would be premature, we emphasize that the above estimate shows that this situation is totally conceivable. This problem will be addressed in more detail in our ongoing work.

The idea that a nearly Einstein-deSitter cosmological model with a low value of the Hubble constant has the potential to fit observations is not new (see e.g. Bartlett et al. 1995). However, our studies clearly demonstrate that reconciling this model with the highest precision cosmological observations to date requires modification of the standard mapping between the cosmological redshift and cosmic scale factor.

An alternative way to reconcile an Einstein-deSitter model with observations was recently proposed by Rácz et al. (2017) who showed that as low value of the Hubble constant as  $h = 0.4$  can be amplified to the observed value



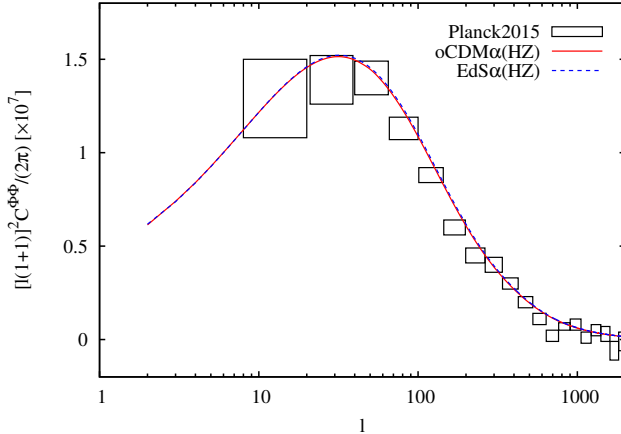


**Figure 8.** Lensing potential power spectrum measured by Planck compared to best-fitting models with redshift remapping and open ( $\Lambda$ CDM $\alpha$ ) or flat (EdS $\alpha$ ) cosmological model. Both models are constrained by the CMB temperature power spectrum from Planck observations (HZ data set).

$h_{\text{obs}} = 0.73$  when the standard FLRW expansion is replaced by the local expansion rate averaged over cosmic space. The similarity between this approach and redshift remapping in terms of amplifying the Hubble constant makes us think whether there is a deeper connection between both models. Future work shall shed more light on this issue.

### 6.3 Lensing

Both open and flat model with redshift remapping require the suppression of the standard lensing potential to fit the temperature power spectrum. In both cases, the amplitude of the lensing potential is 35% smaller at a  $5\sigma$  confidence level than the standard amplitude computed for the corresponding cosmological models. As a sanity check, in Fig. 8 we compare the lensing power spectrum measured from Planck observations (Planck Collaboration et al. 2016c) to the power spectrum of best-fitting models constrained by the HZ data (with  $A_L \approx 0.64$ ) discussed in our work. Since the power spectrum reflects information integrated along the line of sight and thus it is independent of redshift, scaling the multipoles according to redshift remapping is not applicable here and the power spectrum is identical to the output of *camb*.

Fig. 8 demonstrates an excellent agreement between power spectra of best-fitting models and the measurement. It is also straightforward to imagine that using the standard lensing amplitude ( $A_L = 1$ ) would result in a strong tension with the data. Therefore, the suppression of the lensing amplitude appears to be a relevant condition for sustainability of our dark-matter-dominated cosmological fits with redshift remapping. It seems natural to suspect that the suppression of the lensing potential is coupled somehow with redshift remapping. This coupling may be a useful guide in searching for a physical model of redshift remapping.

### 6.4 Age

Observational constraints on dark-matter-dominated models with redshift remapping result in the age of the Universe which does not fall below the lower limits determined from observations of globular clusters and isolated metal-poor stars (Gratton et al. 2003; Bond et al. 2013). Relatively long ages in models with  $\Omega_m \approx 1$  are attained due to low values of the Hubble constant. It shall be regarded as an interesting coincidence that the measured values of  $\Omega_m$  and  $H_0$  in our models always imply the age no smaller than  $\sim 14$  Gyrs. For open models, the age is consistent with its estimate in the Planck cosmological model (see Table 3), but for the EdS model the CMB requires the age larger by 1.3 Gyrs at high confidence level (see Table 4).

The new models modify the age of the Universe at all redshifts. Fig. 9 shows the age of the Universe as a function of the observed redshift. The age is computed using the standard formula incorporating redshift remapping, i.e.

$$t = \int_0^{z_{\text{obs}}[1+\alpha(z_{\text{obs}})]} \frac{dz_{\text{FLRW}}}{(1+z_{\text{FLRW}})H(z_{\text{FLRW}})} \quad (29)$$

For redshifts larger than  $z_{\text{obs}} = 2.5$  (the upper limit of redshift remapping reconstructed from the LZ data set), we assume a simple interpolation between redshift remapping at  $z_{\text{obs}} = 2.5$  and  $z_{\text{obs}} \approx 1100$  (constrained by the CMB). We consider linear and logarithmic interpolations.

For the open model with redshift remapping (left panel in Fig. 9), the current age of the Universe is nearly the same as in the Planck cosmology. However, the new model predicts older Universe at high redshifts than Planck. In particular, the Universe is 10% older at  $z_{\text{obs}} = 2.5$  and, depending on the actual redshift remapping between the current LZ data set and the CMB, it can be 30% older at redshift  $z \sim 10$ . For the EdS model with redshift remapping, the Universe is even older, e.g. 15% older at the present time and up to 60% older at  $z_{\text{obs}} \sim 10$  than in the Planck cosmology.

This general trend of higher estimates of the age in new models with redshift remapping is very interesting in the context of observations of surprisingly well-evolved objects at high redshift such as quasars with supermassive black holes or galaxies with large amount of dust. The existence of such objects poses a challenge to theoretical models describing formation of dust (Gall et al. 2011), supermassive black holes (Mortlock et al. 2011) or first stars and early galaxies in general. Since all well-formed high-redshift objects require unusually rapid formation, it is natural to consider the possibility that this is a global anomaly of the standard  $\Lambda$ CDM cosmological model predicting relatively too strong compression of time at high redshift (Melia 2014). Following this line of reasoning, we notice that our models with redshift remapping have the potential to alleviate this problem, as clearly demonstrated in Fig. 9.

### 6.5 Redshift remapping

The observationally reconstructed redshift remapping increases with the observed redshift. There is also a strong signature that the remapping reaches a plateau at redshift much smaller than the recombination. Using simple extrapolation of redshift remapping reconstructed within the red-

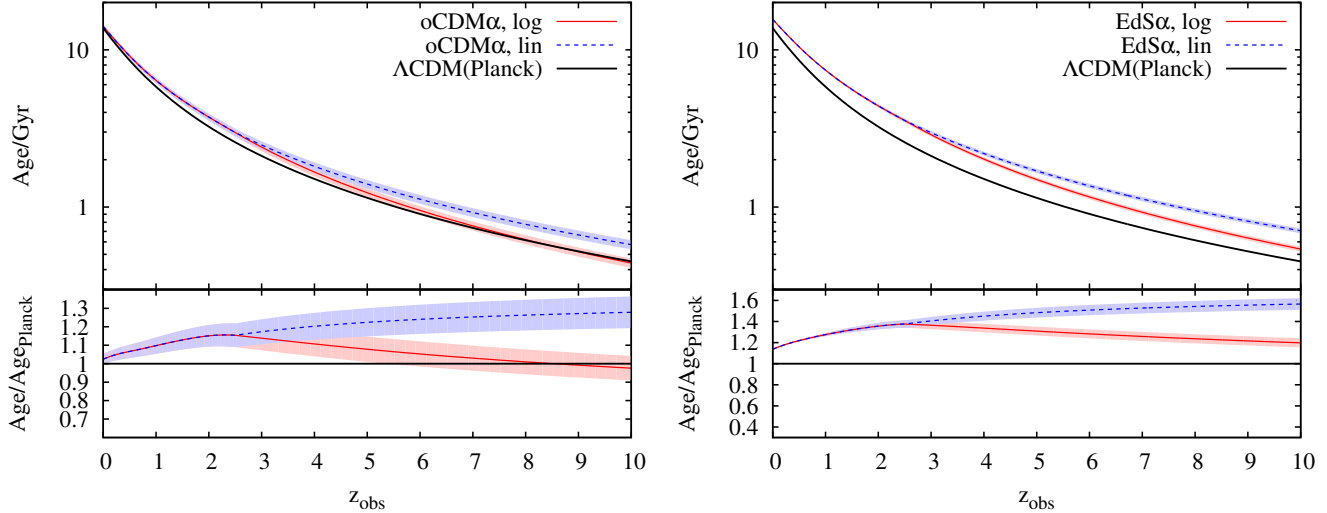


**Figure 9.** The age of the Universe as a function of the observed redshift  $z_{\text{obs}}$  in the open (oCDM $\alpha$ , left panel) and flat (EdS $\alpha$ , right panel) dark-matter-dominated cosmological with redshift remapping. The red and blue lines show results based on logarithmic and linear interpolation between constraints on redshift remapping from the LZ data ( $z_{\text{obs}} \leq 2.5$ ) and the HZ data set ( $z_{\text{obs}} \approx 1100$ ), respectively. The bottom panels show the ratio of the age in the new models to the corresponding age in the Planck  $\Lambda$ CDM cosmology.

shift range of the LZ data set, we find that this plateau begins at  $z_{\text{obs}} \approx (5 - 10)$  for the open model.

Our approach has a status of a phenomenological model and thus we do not intend to address the problem what is a possible physical cause of the reconstructed redshift remapping. There is doubt, however, that the existence of plateau described above implies that any potential physical mechanism should operate only at late epoch of cosmic evolution, although it affects both light from low-redshift objects and the CMB photons. It is tempting to associate this epoch with the growth on highly non-linear structures. In addition, coincidence between the maximum expansion rate in voids and the local value of redshift remapping (which determines the ratio of the actual to locally measured Hubble constant) suggest that the non-linear structures which may play a relevant role here are voids.

Typical models explaining the cosmic acceleration as an effect of a superHubble expansion involves voids whose size exceed substantially the scale of inhomogeneities limited by the BAO. This apparent conflict between the models and observations seems to result from adopting an oversimplified model of void topology. According to recent studies (Falck & Neyrinck 2015; Ramachandra & Shandarin 2017), void as a region without non-linear structures percolates nearly all parts of cosmic space and fills 90-95% of its volume. Such void is infinite (despite a finite scale of the density fluctuations) and, in a way, it functions as a medium for propagation of light in cosmic space. If non-linear evolution generates strong effects on the actual metric, in particular local boosts of the expansion rate demonstrated in recent fully relativistic simulations (Bentivegna & Bruni 2016; Giblin et al. 2016), void can effectively change the standard mapping between the cosmological redshift and cosmic scale factor. The problem whether the resulting redshift remapping can reproduce our non-parametric reconstruction from observations can be addressed in future studies combining recently intro-

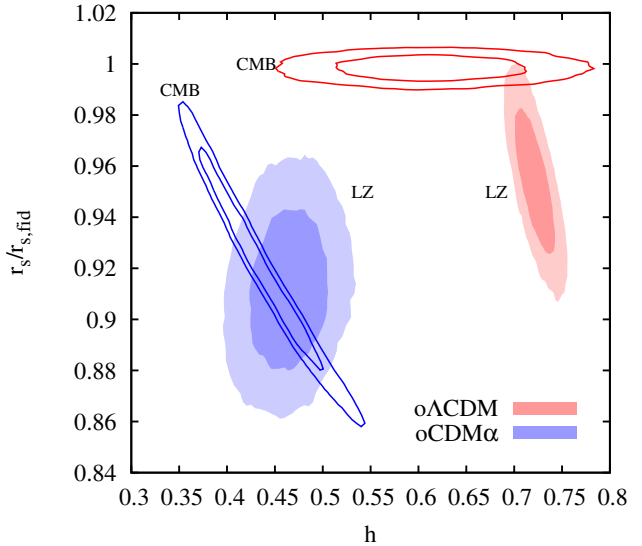


**Figure 10.** The Hubble constant and the BAO scale at low (LZ data set) and high redshifts (HZ data set: CMB) for two cosmological models: open  $\Lambda$ CDM model and open CDM model with redshift remapping. The new CDM model with redshift remapping resolves the discrepancy between the distance scales at low and high redshifts in the standard  $\Lambda$ CDM model.

duced relativistic cosmological simulations with the novel concept of persistently percolating void.

## 6.6 Cosmological distance scales

The new class of models with observationally reconstructed redshift remapping have in general higher degrees of freedom. Therefore, it is not surprising that certain anomalies apparent in the standard  $\Lambda$ CDM model, in particular the

BAO measurements from the Ly- $\alpha$  forest of BOSS quasars, are absorbed by the new models. On the other hand, the consistency between parameters inferred independently from the LZ and HZ data sets should be regarded as a highly non-trivial result. Of particular importance is the consistency between the LZ and HZ observations in terms of the Hubble constant and the BAO scale, two fundamental parameters setting the absolute scales of cosmological distances.

Fig. 10 compares constraints on the Hubble constant and the BAO scale from the LZ and HZ observations assuming two cosmological models: open  $\Lambda$ CDM model and open CDM model with redshift remapping. It is clearly visible that replacing the cosmological constant by redshift remapping eliminates the tension between the distance scales at low and high redshifts, apparent in the standard  $\Lambda$ CDM model. Alleviating this tension without any modification of the standard mapping between the cosmological redshift and cosmic scale factor requires introduction of a dynamical model of dark energy (Di Valentino et al. 2016).

## 7 SUMMARY

We made use of all primary cosmological probes (the CMB temperature power spectrum from Planck observations, Type Ia supernovae, BAO, cosmic chronometers and the local determination of the Hubble constant) to reconstruct a relation between the cosmological redshift  $z_{\text{obs}}$  and cosmic scale factor  $a$  (redshift remapping) and to determine parameters of the assumed dark-matter-dominated cosmological model. Our main findings can be summarized as follows.

- The new cosmological model with redshift remapping provide excellent fits to all data. It eliminates two well-recognized tensions within the standard  $\Lambda$ CDM cosmological model: anomalous values of the BAO signal determined from the Ly- $\alpha$  forest of BOSS quasars and discrepancy between the local and CMB-based determinations of the Hubble constant. All observational signatures of cosmic acceleration are accounted for by the reconstructed redshift remapping instead of dark energy.

- A joint analysis of the CMB temperature power spectrum and low-redshift probes results in a nearly flat cosmological model with  $\Omega_m = 0.87 \pm 0.03$ . When omitting the cosmic chronometer data, the data are consistent with the Einstein-deSitter model.

- Constraints on the Hubble constant and the BAO scale from low-redshift data are fully consistent with those from the CMB temperature power spectrum (respectively 40% and 10% smaller than the standard values in the Planck  $\Lambda$ CDM cosmological model).

- The difference between redshift remapping reconstructed from observations and the standard  $1 + z_{\text{obs}} = 1/a$  relation decreases monotonically with the observed redshift. The reconstructed redshift remapping exhibits the largest deviation from the standard  $a - z_{\text{obs}}$  relation at  $z_{\text{obs}} = 0$  and a plausible constant deviation at  $z_{\text{obs}} \gtrsim 10$ . Both features point to the fact that any possible physical mechanism behind redshift remapping should operate at late times of cosmic evolution.

- The reconstructed redshift remapping predicts a significant difference between the actual and locally measured values of the Hubble constant. This difference coincides with

the maximum expansion rate in cosmic voids formed in the corresponding cosmological model with  $\Omega_m \approx 0.9$ . The actual Hubble constant has sufficiently low value to compensate effects of high dark matter density parameter. In particular, the age of the Universe is  $\sim 14$  Gyrs and is fully compatible with the lower limits determined from astrophysical estimates. Simple interpolations between redshift remapping constrained by the low-redshift probes and the CMB redshift show, however, that the Universe may be up to 30 % older at high redshifts.

- The new cosmological model has a comparable shape of the power spectrum as the standard  $\Lambda$ CDM model. It is nearly indistinguishable from the Planck cosmology in terms of the baryon fraction and the photon-to-baryon number density ratio. The latter guarantees that the newly established model is compatible with the predictions of Big Bang nucleosynthesis.

- Fitting the CMB temperature power spectrum requires the suppression of the standard lensing template by  $\sim 35$  %, both for the open and flat cosmological model. The corrected lensing template is fully consistent with independent measurement of the lensing power spectrum from Planck observations.

### 7.1 Prospects for future tests

The most stringent tests of our model in foreseeable future will rely on increasing the constraining power of low-redshift probes. The primary role will be played by the BAO measurements from the DESI (Levi et al. 2013) and EUCLID (Laureijs et al. 2011) surveys. The future observations of the BAO signal will improve the current status of this probe in several respects: higher precision, filling the current redshift gap at  $0.8 < z_{\text{obs}} < 2.2$ , verification of the BAO anomaly from the Ly- $\alpha$  forest of BOSS quasars and extending the redshift coverage up to  $z_{\text{obs}} = 3.5$  (thanks to the DESI Ly- $\alpha$  forest observations). Precise BAO measurements at high redshifts will be of particular importance, because this is where our model predicts deviations from the standard  $\Lambda$ CDM model (see Fig. 4).

One of the key features of our model is its capability of reconciling the local and CMB-based measurements of the Hubble constant (discrepant when interpreted in the framework of the standard  $\Lambda$ CDM model). From this point of view, future corroboration of the current determination of the Hubble constant in a low-redshift universe will be essential. The best strategy will arguably rely on complementing the measurements based on Type Ia supernovae with other techniques, for example observations of gravitational lens time delays. The accuracy and the precision of the latter method have been substantially improved and the current determinations of the Hubble constant strengthen the tension between the measurements of this parameter in the local and high-redshift universe (Bonvin et al. 2017). The future progress of this measurement will be facilitated by the LSST survey (LSST Dark Energy Science Collaboration 2012) as well as many independent dedicated observational campaigns.

There is no doubt that enabling our model to predict certain subtle observables going beyond basic cosmography will require understanding physics behind redshift remapping. For example, calculating redshift drift (tiny change of the

observed redshifts at the rate  $\sim 10^{-10}$  over a period of 10 years; see Sandage 1962; Loeb 1998) involves evaluating time derivative of redshift remapping what goes beyond predictions of our model at its current phenomenological level. The currently unknown contribution from redshift remapping to redshift drift is the first term in the following expression:

$$\frac{dz_{\text{obs}}}{dt} = -z_{\text{obs}} \frac{d \ln(1 + \alpha)}{dt} + \frac{1}{1 + \alpha} \frac{dz_{\text{FLRW}}}{dt}. \quad (30)$$

Redshift drift will be measured in foreseeable future by the Extremely Large Telescope (ELT) at redshifts  $2 < z_{\text{obs}} < 5$  (Liske et al. 2008) and quite likely by the Square Kilometer Array (SKA) in a complimentary redshift range  $0 < z_{\text{obs}} < 1$  (Abdalla et al. 2015). Bearing in mind that measuring redshift drift is arguably considered the ultimate test of the standard cosmological model, it becomes clear how relevant is to raise the status of cosmological models with redshift remapping to the level of complete physical models.

## ACKNOWLEDGMENTS

The authors thank an anonymous referee for the constructive comments and suggestions. RW acknowledges support through the Porat Postdoctoral Fellowship. RW is grateful for the hospitality of Dark Cosmology Centre where a part of this study was accomplished. FP thanks the support from the MINECO grant AYA2014-60641-C2-1-P.

## REFERENCES

- Abazajian K. N. et al., 2009, *ApJS*, 182, 543  
 Abdalla F. B. et al., 2015, *Advancing Astrophysics with the Square Kilometre Array (AASKA14)*, 17  
 Alam S. et al., 2015, *ApJS*, 219, 12  
 Alam S. et al., 2016, *ArXiv e-prints* 1607.03155  
 Alfaro J., 2012, *Physics Letters B*, 709, 101  
 Alfaro J., González P., 2013, *Classical and Quantum Gravity*, 30, 085002  
 Bartlett J. G., Blanchard A., Silk J., Turner M. S., 1995, *Science*, 267, 980  
 Bassett B. A., Fantaye Y., Hložek R., Sabiu C., Smith M., 2013, *ArXiv e-prints* 1312.2593  
 Bentivegna E., Bruni M., 2016, *Physical Review Letters*, 116, 251302  
 Bernal J. L., Verde L., Riess A. G., 2016, *JCAP*, 10, 019  
 Bernardeau F., van de Weygaert R., Hivon E., Bouchet F. R., 1997, *MNRAS*, 290, 566  
 Betoule M. et al., 2014, *A&A*, 568, A22  
 Beutler F. et al., 2011, *MNRAS*, 416, 3017  
 Blondin S. et al., 2008, *ApJ*, 682, 724  
 Bond H. E., Nelan E. P., VandenBerg D. A., Schaefer G. H., Harmer D., 2013, *ApJ*, 765, L12  
 Bonvin V. et al., 2017, *MNRAS*, 465, 4914  
 Brax P., van de Bruck C., Davis A.-C., Shaw D. J., 2008, *Phys. Rev. D*, 78, 104021  
 Calabrese E., Slosar A., Melchiorri A., Smoot G. F., Zahn O., 2008, *Phys. Rev. D*, 77, 123531  
 Carlberg R. G., Yee H. K. C., Ellingson E., 1997, *ApJ*, 478, 462  
 Carroll S. M., 2001, *Living Reviews in Relativity*, 4  
 Ceron-Hurtado J. J., He J.-h., Li B., 2016, *Phys. Rev. D*, 94, 064052  
 Clifton T., Dunsby P. K. S., 2015, *Phys. Rev. D*, 91, 103528  
 Clifton T., Ferreira P. G., 2009, *Phys. Rev. D*, 80, 103503  
 Clifton T., Ferreira P. G., O'Donnell K., 2012, *Phys. Rev. D*, 85, 023502  
 Delubac T. et al., 2015, *A&A*, 574, A59  
 Di Valentino E., Melchiorri A., Silk J., 2016, *Physics Letters B*, 761, 242  
 Ellis G. F. R., Poltis R., Uzan J.-P., Weltman A., 2013, *Phys. Rev. D*, 87, 103530  
 Etherington I. M. H., 1933, *Philosophical Magazine*, 15  
 Falck B., Neyrinck M. C., 2015, *MNRAS*, 450, 3239  
 Fixsen D. J., 2009, *ApJ*, 707, 916  
 Fixsen D. J., Cheng E. S., Gales J. M., Mather J. C., Shafer R. A., Wright E. L., 1996, *ApJ*, 473, 576  
 Font-Ribera A. et al., 2014, *JCAP*, 5, 027  
 Gall C., Hjorth J., Andersen A. C., 2011, *A&A Rev.*, 19, 43  
 Giblin J. T., Mertens J. B., Starkman G. D., 2016, *Physical Review Letters*, 116, 251301  
 Gratton R. G., Bragaglia A., Carretta E., Clementini G., Desidera S., Grundahl F., Lucatello S., 2003, *A&A*, 408, 529  
 Green S. R., Wald R. M., 2014, *Classical and Quantum Gravity*, 31, 234003  
 Hogg D. W., 1999, *ArXiv Astrophysics e-prints* astro-ph/9905116  
 Jenkins A., Frenk C. S., White S. D. M., Colberg J. M., Cole S., Evrard A. E., Couchman H. M. P., Yoshida N., 2001, *MNRAS*, 321, 372  
 Jimenez R., Loeb A., 2002, *ApJ*, 573, 37  
 Jimeno P., Broadhurst T., Coupon J., Umetsu K., Lazkoz R., 2015, *MNRAS*, 448, 1999  
 Jones D. H. et al., 2009, *MNRAS*, 399, 683  
 Kazin E. A. et al., 2014, *MNRAS*, 441, 3524  
 Laureijs R. et al., 2011, *ArXiv e-prints* 1110.3193  
 Lavinto M., Räsänen S., Szybka S. J., 2013, *JCAP*, 12, 051  
 Levi M. et al., 2013, *ArXiv e-prints* 1308.0847  
 Lewis A., Challinor A., Lasenby A., 2000, *Astrophys. J.*, 538, 473  
 Liske J. et al., 2008, *MNRAS*, 386, 1192  
 Loeb A., 1998, *ApJ*, 499, L111  
 LSST Dark Energy Science Collaboration, 2012, *ArXiv e-prints* 1211.0310  
 Luzzi G., Génova-Santos R. T., Martins C. J. A. P., De Petris M., Lamagna L., 2015, *JCAP*, 9, 011  
 Mantz A. B. et al., 2015, *MNRAS*, 446, 2205  
 Melia F., 2014, *AJ*, 147, 120  
 Meures N., Bruni M., 2012, *MNRAS*, 419, 1937  
 Moresco M., 2015, *MNRAS*, 450, L16  
 Moresco M. et al., 2012, *JCAP*, 8, 006  
 Mortlock D. J. et al., 2011, *Nature*, 474, 616  
 Parkinson D. et al., 2012, *Phys. Rev. D*, 86, 103518  
 Perlmutter S. et al., 1999, *ApJ*, 517, 565  
 Planck Collaboration et al., 2016a, *A&A*, 594, A1  
 Planck Collaboration et al., 2016b, *A&A*, 594, A13  
 Planck Collaboration et al., 2016c, *A&A*, 594, A15  
 Rácz G., Dobos L., Beck R., Szapudi I., Csabai I., 2017, *MNRAS*, 469, L1  
 Ramachandra N. S., Shandarin S. F., 2017, *MNRAS*, 467, 1748

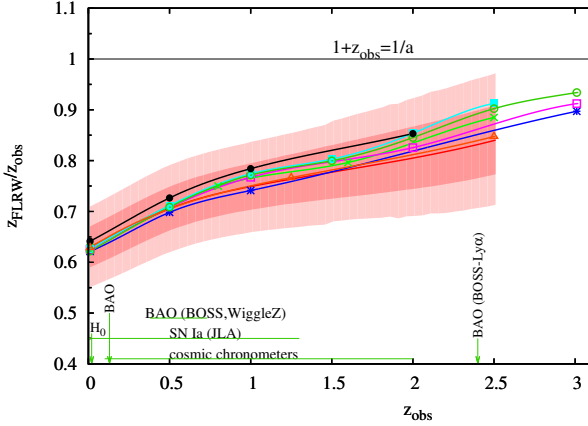


**Figure A1.** Effect of binning defining the knots of the interpolation on best-fitting profile of redshift remapping inferred from the LZ data. The red contours show marginalized 68% and 95% confidence level constraints from our main analysis. Solid lines show best-fitting profiles obtained for several different versions of binning and the symbols indicate the positions of the interpolation knots. All profiles lie well within the 68% confidence level envelope of the main results.

- Räsänen S., Väliiviita J., Kosonen V., 2016, JCAP, 4, 050  
 Riess A. G. et al., 1998, AJ, 116, 1009  
 Riess A. G. et al., 2016, ApJ, 826, 56  
 Ross A. J., Samushia L., Howlett C., Percival W. J., Burden A., Manera M., 2015, MNRAS, 449, 835  
 Sadeh I., Feng L. L., Lahav O., 2015, Physical Review Letters, 114, 071103  
 Sahni V., Shafieloo A., Starobinsky A. A., 2014, ApJ, 793, L40  
 Sandage A., 1962, ApJ, 136, 319  
 Saro A. et al., 2014, MNRAS, 440, 2610  
 Simon J., Verde L., Jimenez R., 2005, Phys. Rev. D, 71, 123001  
 Stern D., Jimenez R., Verde L., Kamionkowski M., Stanford S. A., 2010, JCAP, 2, 008  
 The Dark Energy Survey Collaboration, 2005, ArXiv Astrophysics e-prints  
 Visser M., 2015, Classical and Quantum Gravity, 32, 135007  
 Wojtak R., Hansen S. H., Hjorth J., 2011, Nature, 477, 567  
 Wojtak R., Prada F., 2016, MNRAS, 458, 3331

## APPENDIX A: EFFECT OF BINNING

Here we demonstrate that our choice of binning adopted for the interpolation do not affect robustness of our results. Fig. A1 shows best-fitting profiles obtained for several different ways of binning (with different bin sizes, number of bins and the position of the last bin). All profiles lie well within the error envelope of the main constraints and the cases with an increased number of bins do not reveal any additional features of redshift remapping.